energies

MDPI

Review

Review of High-Torque Electric Machines Applied in Biorobotics and Wearable Devices

Michal Cichowicz [1,*], Marcin Wardach [1,*] and Pawel Wojciech Herbin [2]

[1] Department of Electrical Machines and Drives, Faculty of Electrical Engineering, West Pomeranian University of Technology in Szczecin, 70-310 Szczecin, Poland
[2] Department of Robotics and Control, Faculty of Mechatronics and Electrical Engineering, Maritime University of Szczecin, 71-650 Szczecin, Poland; p.herbin@pm.szczecin.pl
* Correspondence: michal.cichowicz@zut.edu.pl (M.C.); marcin.wardach@zut.edu.pl (M.W.)

Abstract

Nowadays, the market for wearable devices and biorobotics is growing rapidly. In active prostheses and exoskeletons, joints are typically driven by electric machines. The critical challenge is balancing the generated torque with the size and mass of the motor, ensuring the overall weight does not hinder the user's mobility. This paper presents a comprehensive review of high-torque electric machines based on an analysis of 162 publications, primarily from the last decade. The study systematically compares geometric, electrical, and efficiency parameters across various electromechanical converters to identify the optimal limits for bionic applications. Data suggests that an electric machine aiming to align with typical biorobotic requirements would likely fall within an outer diameter of 150 mm, an axial length of 85 mm, and a mass of 1200 g. Furthermore, the required parameters for advanced applications include an efficiency above 95%, a safe nominal voltage of up to 48 V, and the ability to generate torques up to 65 Nm. The analysis highlights that while conventional motors (such as BLDC and PMSM) dominate the market, achieving a torque density exceeding 35–45 Nm/kg—necessary to approach biological muscle capabilities—often requires adopting emerging topologies, such as magnetic gears or Vernier machines. This review provides clear quantitative guidelines for engineers designing optimal drive systems for biorobotics and wearable devices.

Keywords: high torque electric machine; biomechanics; biorobotics

1. Introduction

The dynamic development of modern engineering, especially in areas such as bionic robotics, places increasingly higher demands on electrical machine designers. The key challenge is not only to maximize energy efficiency, but above all to optimize power density and torque while minimizing the weight and size of the devices. In the era of miniaturization and the pursuit of high-dynamic drive systems, the classic approach to electrical machine design is giving way to advanced topologies that better respond to the specific needs of modern applications. The inspiration for this review stems from the direct market need to present clear standards for the design and selection of appropriate electric drive topologies for devices such as exoskeletons, bionic prostheses, and robots built to resemble living organisms.

While existing literature provides extensive reviews on the general operation of electric machines or focuses specifically on control algorithms for prostheses, there is a distinct lack

Check for updates

Academic Editor: José Matas

Received: 24 April 2026
Revised: 27 May 2026
Accepted: 2 June 2026
Published: 10 June 2026

Copyright: © 2026 by the authors. Licensee MDPI, Basel, Switzerland. This article is an open access article distributed under the terms and conditions of the Creative Commons Attribution (CC BY) license.

of comprehensive reviews that synthesize pure engineering parameters (such as torque density, outer diameter, and mass limits) with the stringent physical constraints of wearable biomechanical applications. Previous reviews often treat the electric motor as a generic component, leaving a significant gap regarding clear, quantitative engineering guidelines for optimal motor selection and scaling.

To address this gap, this review aims to answer the following specific research questions:

1. What are the definitive geometric and mass boundaries for electric machines to maintain anthropomorphism and user comfort in bionic applications?
2. What are the necessary quantitative parameters (e.g., torque density, efficiency) required to approximate the performance of biological muscles and joints?
3. At what technological threshold do conventional motor topologies (such as standard BLDC or PMSM) reach their miniaturization limits, necessitating the transition to emerging, high-torque-density technologies (e.g., Vernier machines, magnetic gears)?

The main contribution of this paper is to provide engineers and researchers with a clear, quantitative benchmark for selecting and designing electromechanical converters that perfectly align with the rigorous demands of modern biorobotics.

This article presents a comprehensive comparative analysis of a wide range of electric machines, based on a detailed review of current literature data. The main objective of the study is to systematize geometric, electrical, and performance parameters, allowing for an objective assessment of the technical capabilities of various types of designs—from standard permanent magnet synchronous motors (PMSM) to innovative solutions such as axial flux machines (AFPM), electromechanics energy converters with integrated magnetic gears (MG) and others.

In selecting the literature on the subject, particular attention was paid to publications issued mainly within the last 10 years. This time limit was imposed by the need to verify the relevance of the analyzed solutions in the context of dynamic technological progress. The field of biomechanical drives and mechatronics is developing rapidly, and solutions considered innovative a decade ago may now be giving way to newer technologies with significantly better performance and size parameters.

Keywords used during the review writing were: Bionic Prosthesis, Lower Limb Exoskeleton, Humanoid Robot, Anthropomorphic Hand, Wearable Robotics, Rehabilitation Robot, High Torque Motor, PMSM, BLDC Motor, Axial Flux Motor, Vernier Machine, Flux Switching Machine, Series Elastic Actuator, Torque Density.

The systematic literature selection process was conducted in accordance with PRISMA guidelines to ensure methodological rigor. We utilized major scientific databases, including IEEE Xplore, ScienceDirect, and MDPI, to identify relevant studies published within the last decade. The initial search query employed the keywords mentioned above. Inclusion criteria were defined as: (1) peer-reviewed journal articles, (2) focus on electromechanical drive performance, and (3) available quantitative data on motor parameters. Exclusion criteria encompassed non-English publications and irrelevant studies, such as dental instruments or triboelectric nanogenerators, which were systematically removed during the screening phase. This process yielded a final collection of 162 high-quality peer-reviewed articles utilized for this comparative analysis. Table 1 presents a summary of the results.

Table 1. Literature selection process summary.

Stage	Description	Results
Databases	IEEE Xplore, ScienceDirect, MDPI	-
Search Queries	"Bionic Prosthesis" OR "Lower Limb Exoskeleton" OR "Humanoid Robot" OR "Anthropomorphic Hand" OR "Wearable Robotics" OR "Rehabilitation Robot" AND "High Torque Motor" OR "PMSM" OR "BLDC Motor" OR "Axial Flux Motor" OR "Vernier Machine" OR "Flux Switching Machine" OR "Series Elastic Actuator" OR "Torque Density"	300
Screening	Title and abstract review; removal of duplicates and non-English papers	210
Eligibility	Full-text assessment (exclusion of dental instruments, TENG sensors, and purely theoretical studies)	185
Final Selection	Final review of quantitative data completeness and peer-review quality	162

2. Technological Trends and Performance Analysis of High-Torque Electric Machines in Biomechanics

The development of drives for biomechanical devices is characterized by a continuous struggle between the high-torque, low-speed requirements of biological joints and the inherent high-speed, low-torque nature of conventional electric motors. Rather than merely classifying machines by their construction, modern literature categorizes them based on their integration paradigms: heavily geared conventional drives versus emerging high-torque-density direct drives.

Many of the biomechanical devices contain electrical machines for very different usage. The most common machines are the servo motors; hence, closed drive system composed of direct current (DC) motor or brushless direct current (BLDC) motor with a ready implemented encoder. The servomotor rotates, causing feedback pulses to be sent from the encoder to the servo amplifier. The deviation counter subtracts the feedback pulses from the encoder from the command pulses from the positioning module. The pulses counted by the deviation counter are called error pulses.

Sometimes the scientists decide to use DC motors (Figure 1), because of their size, weight and easiness of control. They are the machines in which electrical energy from a voltage source is converted into mechanical energy in the form of continuous rotational motion. Usually they can be used with additional gearbox to increase the torque on a shaft, which is very needed for demanded biomechanical constructions.

Another type of electrical machines are BLDC motors (Figure 2). The rotor moves relatively frictionless with the stator. This approach offers engineers several advantages. The absence of brushes and their accompanying friction and sparking makes the BLDC motor reliable, as it requires little or no maintenance and has a longer service life. In some works it is possible to find BLDC motors with additional gearboxes (i.e., harmonic or planetary gearbox) to increase the torque—similarly to DC motors and other constructions.

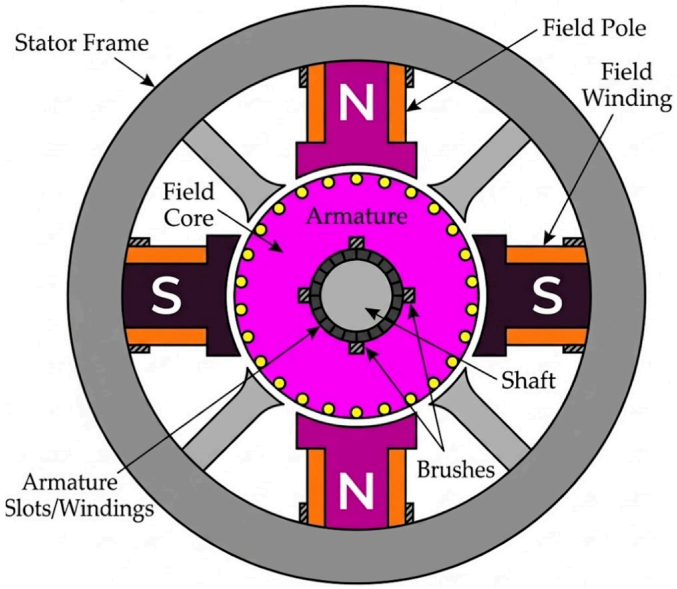


Figure 1. DC motor.

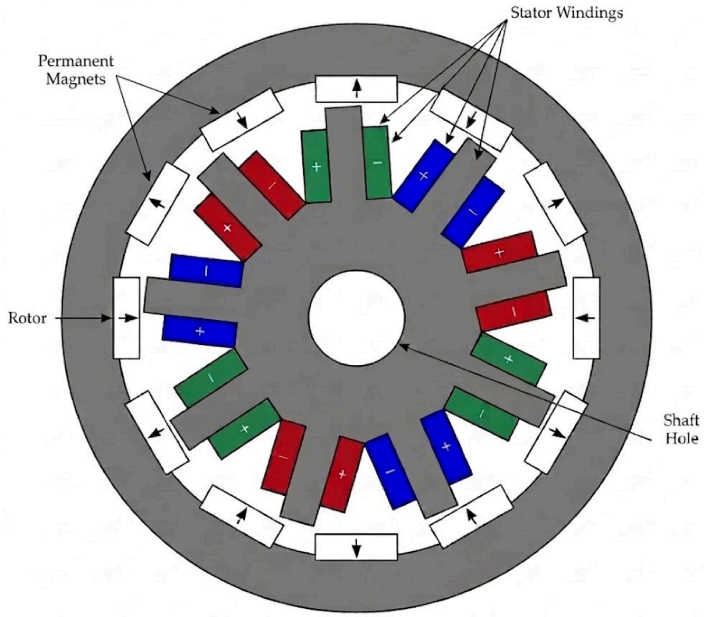


Figure 2. BLDC motor.

Occasionally, it is possible to find a stepper motor in some biomechanical implementations. A basic stepper motor (Figure 3) consists of a rotor and a stator, which only in name are the components that link steppers to traditional DC motors, as the design of these parts is quite different in the two types of motors. Stepper motors, unlike motors that perform a constant rotational motion, are brushless motors. They do not have mechanical-electrical components working with a commutator to force current to flow in the relevant parts of the rotor winding.

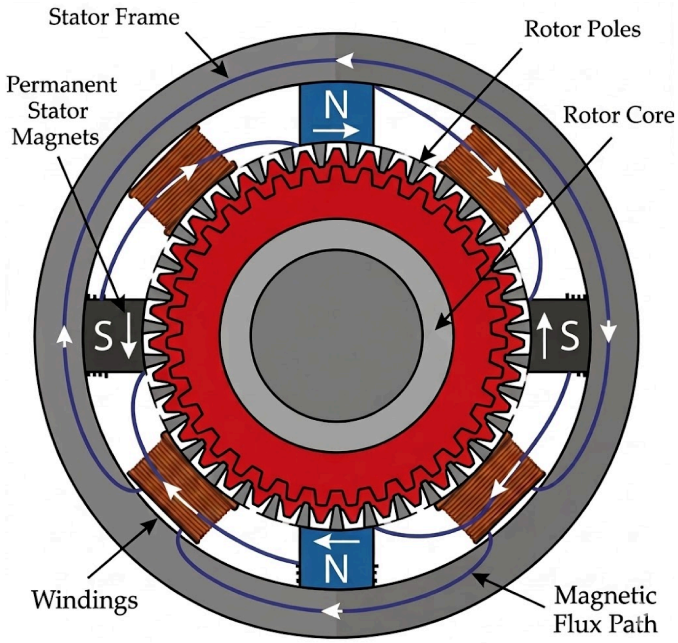


Figure 3. Stepper motor.

The most interesting types of electrical machines implemented in biomechanical devices are High Torque (HT) motors. The idea of them in biomechanical constructions is to help, i.e., a potential heavy patient in a rehabilitation with huge range of controllable torque. In some of them, the magnetic gearbox is used to increase the value of the torque.

Some of the biomechanical constructions are equipped in Permanent Magnet Synchronous Motors (PMSM). Permanent Magnet Synchronous Motor (Figure 4) works by using magnets on its rotor and a magnetic field created by electricity in its stator. When an AC power is sent to the stator, it creates a rotating magnetic field. The rotor, with its permanent magnets, aligns with this field and rotates at the same speed. This synchronized rotation produces torque, which turns the motor shaft and powers whatever the motor is connected to. PMSMs are efficient and commonly used in electric vehicles and appliances.

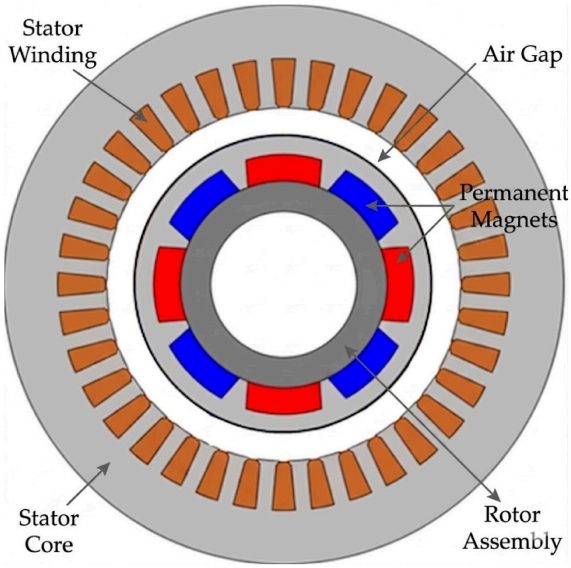


Figure 4. Permanent Magnet Synchronous Motor (PMSM).

There are also other electric machines proposed in literature, that in the authors opinion are relevant to comment and can be used in biomechanical constructions in the future works.

Historically, biomechanical devices have heavily relied on classic Direct Current (DC), Brushless DC (BLDC), and standard Permanent Magnet Synchronous Machines (PMSM). Their widespread adoption stems from technological maturity, ease of control, and high individual efficiencies. However, their direct application in wearable robotics faces a fundamental physical limitation. The electromagnetic torque T_e generated by a conventional radial-flux machine is strictly constrained by its rotor volume, as described by the classical machine sizing equation:

$$T_e = \frac{\pi}{4} \cdot k \cdot D^2 \cdot L$$

where D is the rotor diameter, L is the active axial length, and k represents the machine constant (which depends on the specific magnetic and electrical loadings).

Because the strict geometric limits of prostheses and exoskeletons severely restrict both D and L, conventional motors cannot generate the 30–65 Nm required for human locomotion directly. To bridge this gap, designers invariably couple these motors with high-ratio mechanical transmissions (e.g., harmonic or planetary gearboxes). While this multiplies the torque, it introduces significant drawbacks. The overall system efficiency η_{sys} is penalized by the mechanical losses of the gearbox:

$$\eta_{sys} = \eta_{motor} \cdot \eta_{gear}$$

As mechanical gearboxes typically introduce 5–15% losses, the system efficiency drops, increasing the thermal load and draining battery life. Furthermore, high gear ratios exponentially increase the reflected rotor inertia and introduce friction, effectively destroying the system's backdrivability—a critical safety feature in human–robot interaction that allows the user to back-drive the joint during a fall or sudden movement.

Some publications are responding to Synchronous Reluctance (SynRel) motors (Figure 5). A SynRel motor operates by using magnetic resistance, or reluctance, in its rotor to generate movement. In this motor, the stator produces a rotating magnetic field when powered by alternating current. The rotor, unlike in other motors, does not have any magnets or windings; instead, it is made of iron with carefully designed air gaps or low-magnetic sections. These gaps create paths for the magnetic field, and as the stator's field rotates, the rotor aligns itself to minimize magnetic resistance. This alignment generates torque, causing the rotor to spin at the same speed as the stator's magnetic field.

The Flux Switching Permanent Magnet (FSPM) Motors are also relevant to comment (Figure 6). An FSPM motor is a type of motor that uses permanent magnets and a unique stator design to produce torque. In an FSPM motor, the magnets are placed on the stator rather than on the rotor. The stator also has windings that, when powered by AC current, create magnetic fields that interact with the magnets. As the current in the windings switches direction, the magnetic flux changes paths, creating a force that pulls the rotor into alignment. This "flux-switching" effect drives the rotor to turn and produce mechanical motion. Because the magnets stay on the stator, they are better protected, which can increase the motor's durability. FSPM motors are known for their high torque density, efficiency, and reliability, making them useful in many industrial applications.

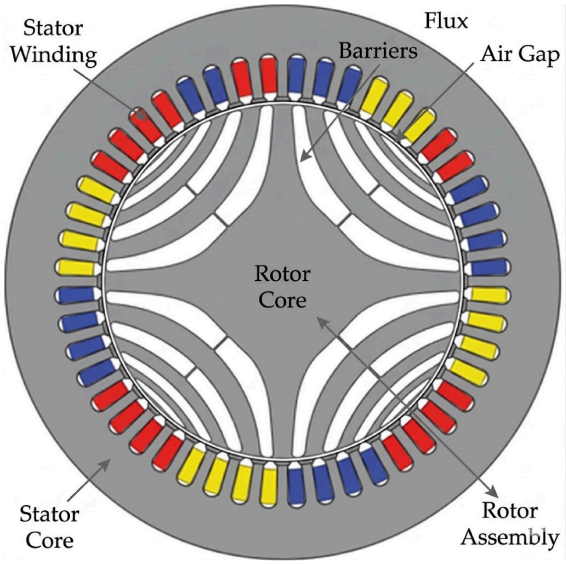


Figure 5. SynRel motor.

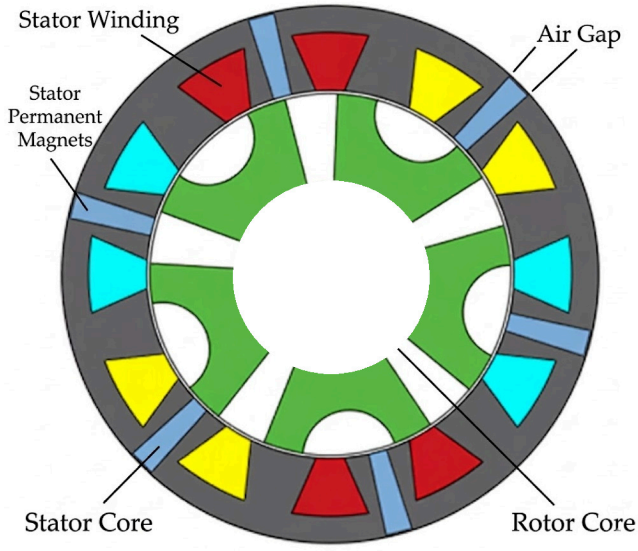


Figure 6. Flux Switching Permanent Magnet (FSPM) Motor.

Sometimes the scientists are building Permanent Magnet Vernier Motors (PMVM). A PMVM (Figure 7) is a type of motor that combines permanent magnets and a unique gear-like magnetic structure to produce high torque at low speeds. In a PMVM, both the stator and rotor contain specially arranged magnetic poles. Permanent magnets are usually mounted on the rotor, while the stator has windings that create a magnetic field when energized by alternating current. The key feature of a PMVM is its "magnetic gearing" effect: the motor's magnetic structure allows the rotor to rotate at a slower speed than the stator's magnetic field, similar to a mechanical gear reduction. This design enables the motor to generate high torque even at low speeds, making it highly efficient and useful in direct-drive applications. PMVMs are often used in applications where high torque at low rotational speeds is needed, such as in electric vehicles, robotics, and wind energy systems.

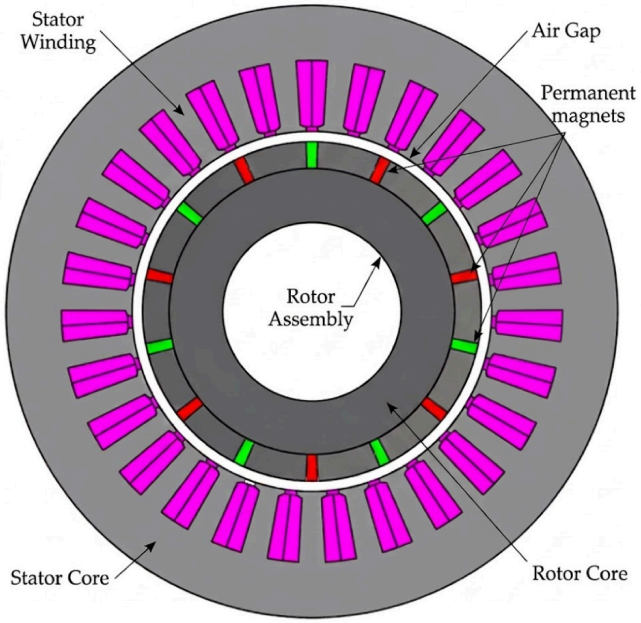


Figure 7. Permanent Magnet Vernier Motors (PMVM).

If we need to optimize the cost of manufacturing of electric machines, the Switched Reluctance Machines (SRM) are worth discussing. An SRM (Figure 8) works by using the magnetic reluctance of its rotor to generate motion. Unlike other types of motors, an SRM does not have permanent magnets or windings on the rotor. Instead, it relies on the rotor's iron structure, which is shaped to create areas of varying reluctance. In an SRM, the stator has coils that are energized in a specific sequence. As the current flows through these coils, a magnetic field is created. The rotor, which has a unique shape with poles that align with the stator's magnetic field, moves to minimize the reluctance, or the magnetic resistance between the stator and rotor. This creates the torque that causes the rotor to turn. Because the rotor only moves to reduce magnetic reluctance, SRMs are simple and robust, with fewer components, making them reliable and cost-effective. However, they require a more complex control system to switch the coils on and off at the right times.

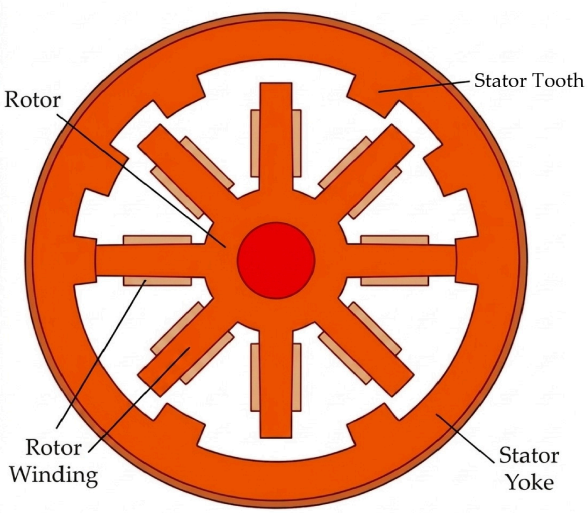


Figure 8. Switched Reluctance Machine (SRM).

The researchers are conducting some experiments using Axial-Flux Permanent Magnet (AFPM) Motors. An AFPM motor (Figure 9), also known as a disc motor, is a type of electric

motor where the magnetic flux flows along the axis of the rotor, rather than radially as in traditional motors. In this design, the stator is typically flat and disc-shaped, and the rotor contains permanent magnets. The magnetic field generated by the stator interacts with the rotor's magnets, creating torque and causing the rotor to spin along its axis. This design results in a motor that is more compact, lighter, and more efficient compared to traditional radial-flux motors. One of the main advantages of AFPM motors is their high power density, meaning they can produce a large amount of power relative to their size and weight. The compact design makes them ideal for applications where space and weight are crucial, such as in electric vehicles and aerospace systems. Additionally, these motors are known for their efficiency and low losses, which contribute to their overall performance.

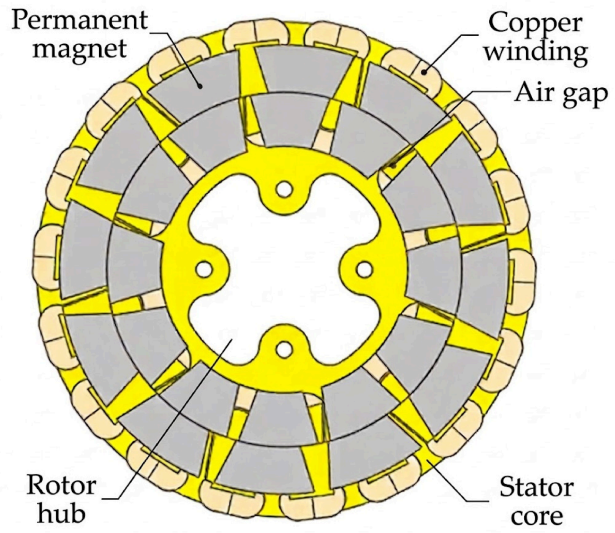


Figure 9. Axial-Flux Permanent Magnet (AFPM) Motor.

One of the proposed publications corresponds to a Yokeless and Segmented Armature (YASA) Motor. The YASA motor design features a stator with separate magnetic poles, each having a single concentrated winding. The rotor is made up of two identical plates arranged 180 electrical degrees apart, with magnets of the same polarity facing each other across the stator. This structure reduces the amount of soft magnetic material used, which helps cut down on losses, weight, and volume, while also lowering manufacturing costs. Additionally, this setup allows for a compact coil with shorter end windings. Compared to other axial-flux and radial-flux motors, the YASA motor offers considerable cost savings. However, due to the relatively long air gaps in the design, YASA motors tend to have low self-inductance, which can lead to high short-circuit currents. While this can present challenges for fault-tolerant designs, it also provides an advantage in applications requiring quick changes in torque, such as torque vectoring, due to the motor's low time constant. The construction is similar to APFM.

To overcome the limitations of mechanical transmissions, a distinct trend in recent literature is the shift towards Quasi-Direct Drive (QDD) and pure Direct Drive (DD) paradigms. This shift necessitates the use of unconventional machine topologies that maximize torque density ρ_T :

$$\rho_T = \frac{T_{max}}{m}$$

where T_{max} is the peak electromagnetic torque and m is the active mass of the machine. Reaching the threshold of 35–45 Nm/kg, which is necessary to approximate biological muscle capabilities, requires fundamentally different magnetic architectures.

- Axial-Flux Permanent Magnet (AFPM) and YASA Motors: Unlike radial machines, AFPM motors direct the magnetic flux parallel to the axis of rotation. This pancake-like geometry drastically increases the effective air-gap radius, yielding higher torque for the same mass. While YASA (Yokeless and Segmented Armature) designs push this even further by eliminating the stator yoke to save weight, their large diameters often exceed the strictly defined limits (e.g., <150 mm) for anthropomorphic applications.
- Flux Modulation and Vernier Machines (PMVM, FSPM): Another emerging trend is the integration of the "magnetic gearing" effect directly into the motor structure. Permanent Magnet Vernier Machines (PMVM) and Flux Switching Permanent Magnet (FSPM) motors utilize a specific stator tooth and rotor pole combination to modulate the magnetic flux. The effective pole pair number of the magnetic field interacting with the stator winding p_s is modulated by the number of rotor segments Z_r and permanent magnet pole pairs p_{pm} :

$$p_s = |Z_r - p_{pm}|$$

This flux modulation allows the rotor to rotate at a fraction of the synchronous speed of the fundamental magnetic field, inherently multiplying the output torque without any physical contact, friction, or mechanical wear.

- Reluctance Machines (SRM, SynRel): Switched Reluctance (SRM) and Synchronous Reluctance (SynRel) motors are also investigated due to their robust, magnet-free rotors, which lower manufacturing costs and eliminate the risk of demagnetization under high peak currents. However, they suffer from higher torque ripple, which can cause undesirable vibrations in wearable devices, necessitating complex non-linear control strategies.

In summary, the literature reveals a clear transition. While BLDC and standard PMSM paired with gearboxes remain the pragmatic choice for current commercial applications, cutting-edge research in biorobotics is heavily focused on AFPM, PMVM, and other flux-modulating topologies. These emerging machines provide the high ρ_T required to eliminate mechanical gearboxes, thereby maximizing efficiency, backdrivability, and dynamic response in human-assistive devices.

In two found publications, the authors decided to prepare the Consequent Pole Flux Reversal Machines (CPFRM). CPFRM (Figure 10) are a type of electric motor that use a unique rotor and stator design to improve efficiency, torque density, and performance. The key feature of these motors is the use of consequent poles on the rotor, where the magnetic poles of the rotor are alternately arranged in such a way that the flux in the rotor reverses as it interacts with the stator. In a Consequent Pole Flux Reversal Machine, the rotor has two sets of poles that are connected to each other in a way that creates a high torque output while minimizing energy losses. This flux reversal occurs because the stator's magnetic field interacts with the rotor's poles in a manner that causes the magnetic flux to "flip" direction during operation. This results in a more efficient use of the permanent magnets on the rotor. The motor's stator typically features concentrated windings that help reduce the amount of copper used and reduce losses, leading to better overall efficiency. Because of the way the rotor poles are arranged and the flux reversal that occurs, CPFRMs can generate high torque and power density while maintaining low energy consumption and a compact form factor. These motors are well-suited for applications where high torque and efficiency are needed in a relatively small and lightweight package.

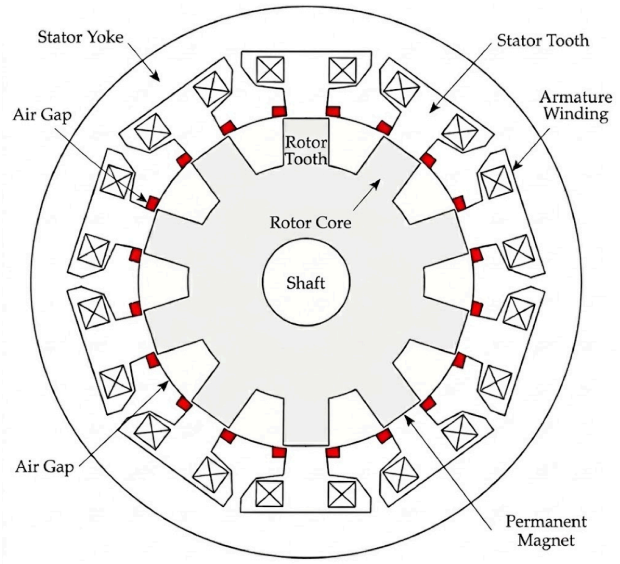


Figure 10. Consequent Pole Flux Reversal Machine (CPFRM).

One of the studies has also presented have also presented a usage of linear motor (Figure 11). A linear motor is a type of electric motor designed to produce linear motion, rather than the rotational motion that traditional motors generate. It works on the same basic principles as a regular electric motor, but instead of a rotating shaft, the motor creates a straight-line movement. In a linear motor, the stator has coils that are energized by an alternating current. These coils create a magnetic field that interacts with the magnets or coils on the moving part, often called the "primary" or "slider." As the stator's magnetic field moves, it pushes or pulls the slider, creating linear motion. The movement can be continuous, and the speed and direction can be controlled by adjusting the timing of the current sent to the coils. These motors offer high efficiency and accuracy because they eliminate the need for mechanical parts like gears or screws, making them ideal for tasks that require smooth and fast movement over a straight path.

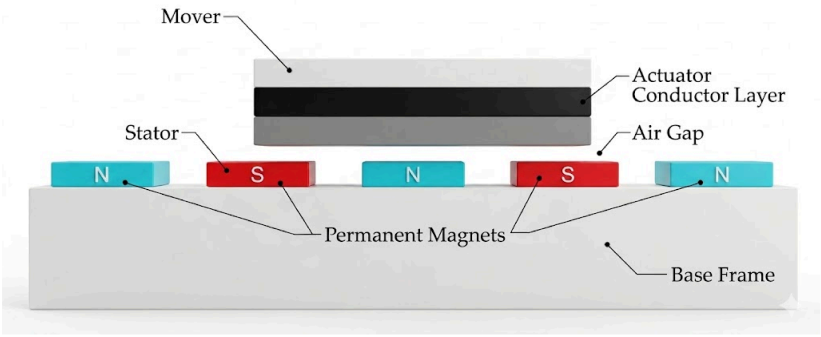


Figure 11. Linear motor.

The last group of motors with high torque found in literature are induction motors (Figure 12). An induction motor is a type of electric motor that operates on the principle of electromagnetic induction. It is one of the most common types of motors used in various industrial and household applications due to its simplicity, durability, and efficiency. In an induction motor, the is supplied with AC which creates a rotating magnetic field. This magnetic field induces a current in the rotor, which then generates its own magnetic field. The interaction between the stator's rotating magnetic field and the rotor's magnetic field causes the rotor to turn. The key feature of an induction motor is that the rotor does not need any external electrical power or permanent magnets. The current is induced

in the rotor by the changing magnetic field from the stator, which is why it is called an "induction" motor. They are known for being reliable, cost-effective, and requiring minimal maintenance because they have no brushes or external power supply to the rotor. However, they are typically less efficient than motors with permanent magnets, especially at lower speeds.

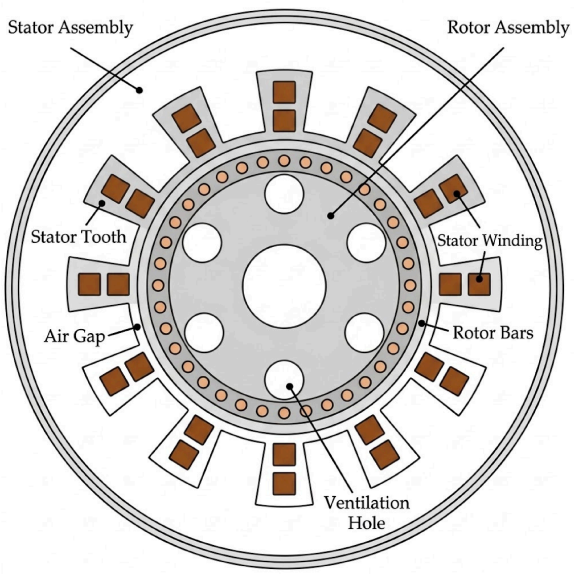


Figure 12. Induction motor.

Table 2 summarizes the fundamental relationships describing the electromagnetic torque (T_e) for the various machine topologies analyzed in this study. This comparison illustrates how torque generation mechanisms differ across topologies, ranging from current-controlled permanent magnet interaction to reluctance-based variation.

Table 2. Literature selection process summary.

Machine Topology	Torque Generation Principle	Torque Dependency (Simplified)
PMSM/BLDC	Interaction between PM flux and stator current	$T_e \propto p \cdot \psi_{pm} \cdot I_q$
SRM	Variation of magnetic reluctance	$T_e \propto \frac{1}{2} i^2 \frac{dL}{d\theta}$
SynRel	Magnetic anisotropy (reluctance difference)	$T_e \propto p(L_d - L_q) i_d i_q$
PMVM	Magnetic flux modulation (gearing effect)	$T_e \propto p_s \cdot \psi_{pm} \cdot I_q$
AFPM	Interaction in the axial air gap	$T_e \propto k \cdot D^2 \cdot L \cdot B_{avg} \cdot A$

The relationships presented in Table 2 elucidate the physical principles underlying the torque production in different machine architectures. While conventional machines like PMSM and BLDC rely on the direct interaction between permanent magnet flux and stator current, reluctance-based machines (SRM, SynRel) generate torque through the rotor's tendency to minimize magnetic resistance, governed by inductance variation. Vernier/PMVM topologies employ flux modulation to effectively multiply the electrical pole-pair interactions, creating a 'magnetic gearing' effect that is particularly advantageous for low-speed, high-torque biorobotic tasks. This analytical summary bridges the gap

between machine construction and performance metrics, providing a deeper understanding of why specific topologies are better suited for demanding biomechanical applications.

Based on the 162 articles adopted in the paper, it was found that the largest number of motors used in bionic designs are BLDC motors (23), servo motors (30), DC motors (13), various high-torque motors (10) and PMSM motors (30). Stepper motors (3) are the most commonly used. Furthermore, considering the other high torque motors on the shaft, it was found that SynRel (2), FSPM (2), PMVM (5), SRM (3), YASA (1), CPFRM (2), AFPM (4), linear (3) or induction (2) motors are referred to in the literature. The entire comparison is presented in Figure 13 and Table 3.

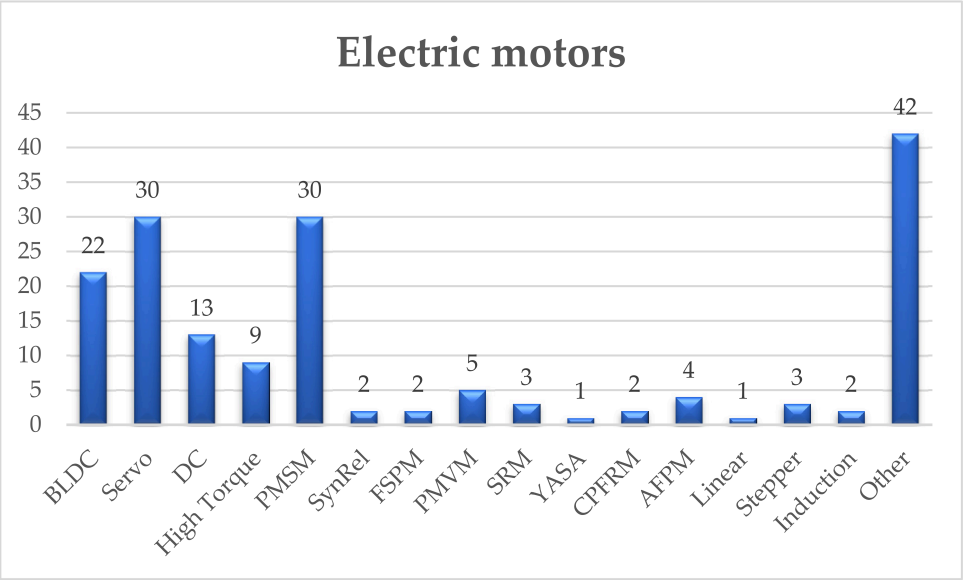


Figure 13. Type of motors with high torque graph of amount.

Table 3. High torque machines.

Machine Type	Number of Publications	Citation
BLDC	22	[1–22]
Servo	30	[23–52]
DC	13	[4,51,53–63]
High Torque	9	[64–72]
PMSM	30	[69–71,73–99]
PMVM	5	[72,100–103]
AFPM	4	[104–107]
SRM	3	[108–110]
Stepper	3	[26,51,111]
FSPM	2	[112,113]
CPFRM	2	[114,115]
Induction	2	[116,117]
Linear	1	[118]
SynRel	2	[79,119]
YASA	1	[120]
Other	42	[121–162]

3. Analysis of the Articles with the Critical Parameters of the Electric Machines

This section examines the critical parameters of electric machines relevant to biomechanical applications. The primary factors include size (outer diameter and axial length), mass, and nominal torque. Secondary parameters are also evaluated, as they determine the auxiliary components required when designing a complete biomechanical drive system. This review focuses on defining practical design boundaries based on literature ranges; statistical averages are omitted due to the high technological diversity of the analyzed research. It is important to emphasize that this review considers both bare electric motors and complete actuator units (incorporating mechanical or magnetic gearboxes). Where data was provided, we have distinguished between the intrinsic motor parameters and the overall drive-train performance, acknowledging that the latter reflects the added weight and efficiency losses of the transmission stage.

3.1. Machine Diameter

During the selection and design of drives dedicated to biomechanical structures, the outer diameter of the electric machine serves as the primary parameter. This restriction is dictated by the absolute necessity to maintain system compactness. Limiting the outer diameter is crucial for preserving the anthropomorphism of the structure; the drive must not protrude beyond the natural outline of the user's limb or joint. This constraint is essential for ensuring both the aesthetic appeal and the functional viability of prostheses and exoskeletons. Furthermore, a minimized diameter facilitates the seamless integration of the drive within the supporting frame, reducing the risk of collision with other mechanical elements. Consequently, minimizing this transverse dimension forms the foundation for all subsequent design phases, directly imposing constraints on other parameters, such as the machine's axial length and its achievable torque. The comparison results are summarized in Table 4.

Table 4. High torque machine diameters.

Machine Diameter (mm)	Machine Example	Publication Example
30–40	DC (foot prosthesis)	[48]
100–110	BLDC (exoskeleton)	[16]
110–120	BLDC (humanoid robot)	[66]
120–130	BLDC (humanoid robot)	[66]
140–150	Motor with Halbach magnetic gearbox (no info about application)	[75]
>150	YASA (d = 380 mm, cars)	[120]

An analysis of available solutions and current literature defines typical dimensional ranges for drives in biomechanical engineering. The most frequently utilized motors in these designs possess diameters ranging from 30 to 140 mm. However, the literature indicates that for applications demanding exceptionally high torque, units with slightly larger diameters—up to 150 mm—are permissible. It must be explicitly noted that drives exceeding the 150 mm threshold are typically designed for entirely different industrial applications. A prime example is the previously mentioned YASA motor; despite its advanced technology, it is optimized for the automotive industry and, due to its substantial size, remains unsuitable for compact biomechanical designs.

3.2. Machine Length

Another critical geometric parameter is the axial length of the machine. The motor must not be excessively long, as an elongated structure would make the device bulky and highly susceptible to mechanical damage. Constraining this dimension guarantees that the drive module remains within the natural anatomical boundaries of the limb. An oversized drive module could lead to environmental collisions or interfere with the user's opposing limb during the gait cycle. Additionally, it would negatively impact the overall ergonomics and aesthetics of the device, ultimately compromising its anthropomorphic nature. The comparison results are summarized in Table 5.

Table 5. High torque machine lengths.

Machine Length (mm)	Machine Example	Publication Example
35–40	BLDC (exoskeleton)	[16]
40–45	BLDC (humanoid robot)	[66]
70–75	Cylindric drive (exoskeleton)	[16]
80–85	DC (prosthesis)	[48]
>100	YASA (125 mm, cars)	[120]

The analysis demonstrates that in prosthetic applications, the axial length of drive units typically reaches a maximum of 85 mm, establishing the upper limit for solutions integrated directly into artificial limbs. Drives exceeding 100 mm in length are categorically reserved for larger-scale industrial applications. Exceeding this dimensional constraint generally disqualifies a motor from wearable biomechanical use, as it compromises the mandatory compactness and ergonomic integrity of the system.

3.3. Machine Mass

The mass of the drive unit is just as critical as its geometric dimensions. In biomechanical engineering, weight minimization is a top priority, directly influencing the user's metabolic energy expenditure and overall comfort. Excessive weight accelerates user fatigue and significantly increases the system's moments of inertia. This factor is particularly critical for drives mounted on the distal segments of limbs; any additional mass placed far from the anatomical axis of rotation severely impairs movement dynamics and complicates precise control. The comparison results are summarized in Table 6.

Table 6. High torque machine masses.

Machine Mass [g]	Machine Example	Publication Example
0–300	BLDC (humanoid robot)	[43]
300–600	BLDC with harmonic gearbox (exoskeleton)	[105]
600–900	BLDC (exoskeleton)	[16]
900–1200	BLDC (humanoid robot)	[66]
>1200	Huge axial magnetic gearbox setup (6.6 kg)	[75]

A review of the available literature indicates that the mass of individual drives in standard biomechanical designs generally does not exceed 1200 g. This value represents a pragmatic limit that preserves device functionality. While significantly heavier integrated drive units exist—weighing up to 6.6 kg—their implementation carries substantial risks.

Such massive loads can destabilize the entire physical structure, drastically impairing dynamic performance and hindering the user's ability to maintain balance.

3.4. Machine Efficiency

Energy efficiency represents another fundamental parameter. In mobile designs constrained by limited battery capacities, high efficiency is essential to ensure adequate device autonomy and to extend the operational duration per charge cycle. This parameter also dictates thermal management strategies; energy losses within the motor are inherently converted into heat. Because biomechanical drives operate in close proximity to human tissue, minimizing heat generation is paramount for user safety and comfort, simultaneously eliminating the need for heavy, complex active cooling systems. The comparison results are summarized in Table 7.

Table 7. High torque machine efficiencies.

Machine Efficiency [%]	Machine Example	Publication Example
90–95	BLDC/DC (humanoid, exoskeleton)	[16,66]
75–85	Drive with additional gearbox (prostheses, exoskeleton)	[4]

The analysis reveals that bare BLDC or DC motors utilized in these applications exhibit excellent efficiency, typically ranging from 90% to 95%. However, a significant discrepancy arises when analyzing complete drive units equipped with high-ratio mechanical transmissions. In geared systems, unavoidable friction losses within the reducer components drastically decrease overall efficiency, yielding performance metrics substantially lower than those of the standalone electric motor.

3.5. Machine Power

Nominal power defines the continuous operational capability of a drive system and correlates directly with its thermal management. In biomechanical applications, determining this value requires a careful compromise between facilitating high motion dynamics and maintaining compact hardware dimensions. Although human biomechanics frequently necessitate momentary operation in an overload state (e.g., during sit-to-stand transitions or stair climbing), the continuous nominal power must safely accommodate the average energy demands of typical walking cycles to prevent winding overheating. Insufficient nominal power leads to rapid thermal accumulation, which, in wearable robotics, compromises both user safety and hardware longevity. The comparison results are summarized in Table 8.

Table 8. High torque machine nominal powers.

Machine Power [W]	Machine Example	Publication Example
0–50	BLDC (humanoid)	[51]
50–100	Servo (prosthesis)	[31]
100–150	DC (zoomorphic robot)	[62]
150–200	Servo (humanoid)	[51]
250–300	BLDC (humanoid)	[3]
>500	BLDC (exoskeleton)	[16]

Evaluating the nominal power ratings reveals a clear correlation between the specific biomechanical application and its energy requirements. For lightweight structures, such as prostheses or upper-body humanoid components, power outputs ranging from 0 to 100 W are generally adequate. Conversely, complex humanoid and zoomorphic robots necessitate a higher range of 150–300 W. The highest power demands, frequently exceeding 500 W, are observed in exoskeletons. This is due to their operational mandate to actively assist or fully support the user's body weight, demanding substantially more energy than autonomous prosthetic limbs.

3.6. Machine Torque

Generating high torque is a foundational requirement for biomechanical drives, directly mirroring the characteristics of the human musculoskeletal system, which operates at high forces and relatively low angular velocities. Consequently, torque density—expressed as the ratio of generated torque to the motor's mass or volume—serves as a primary quality indicator. Maximizing torque density enables system miniaturization and facilitates the reduction of mechanical gear ratios. This reduction fundamentally improves overall efficiency and enhances control transparency, specifically backdrivability. Furthermore, peak torque capacity is vital; devices like active prostheses must handle severe, short-term dynamic overloads (e.g., sudden acceleration, stair climbing, or stumble recovery) without risking thermal failure or rotor demagnetization. The comparison results are summarized in Table 9.

Table 9. High torque machine nominal torques.

Machine Torque [Nm]	Machine Example	Publication Example
0–5	Servo (robotic hand)	[23]
15–20	Servo (prosthesis)	[31]
30–35	BLDC (humanoid robot)	[66]
50–55	BLDC (humanoid robot) (other configuration)	[66]
60–65	BLDC (prosthesis)	[110]
>70	YASA (cars)	[120]

The analysis of nominal torque values reveals a clear hierarchy of force requirements depending on the intended biomechanical function. Precision manipulators, such as robotic hands, operate efficiently within the 0–5 Nm range. This demand escalates sharply for limb prostheses; standard solutions require 15–20 Nm, whereas highly dynamic architectures (e.g., active ankle or knee joints) demand 60–65 Nm. Humanoid robots occupy the intermediate spectrum, requiring 30–55 Nm. The data further reinforces the technological applicability limits; drives generating torque beyond 70 Nm (such as the automotive YASA unit) fall outside the practical scope of rehabilitation engineering and biorobotics.

3.7. Machine Voltage

Table 10 confirms the overwhelming preference for safe operating voltages up to 48 V (SELV) in biomechanical designs, dictated by strict human safety regulations and the inherent characteristics of portable battery packs. A clear correlation exists between the application type and voltage level: lightweight prostheses generally operate below 24 V (consuming 50–100 W), whereas heavy-duty exoskeletons and humanoid robots (requiring >500 W) utilize the upper 36–48 V range to maintain optimal efficiency and minimize current draw.

Table 10. High torque machine nominal voltages.

Machine Voltage [V]	Machine Example	Publication Example
<24	Servo (prosthesis)	[45]
24	BLDC (hand orthosis)	[20]
36	DC (prosthesis)	[48]
36–48	BLDC (humanoid robot)	[10]
>48	SRM (other construction)	[110]

3.8. Machine Speed

Because human joints function at relatively low angular velocities, and conventional electric motors are optimized for high-speed operation, standard designs heavily rely on high-reduction gearboxes. However, the contemporary design paradigm for high-torque machines reverses this trend; the primary engineering objective is now to minimize nominal rotational speed in order to maximize direct shaft torque. The comparison results are summarized in Table 11.

Table 11. High torque machine nominal speeds.

Machine Speed [RPM]	Machine Example	Publication Example
0–500	Claw pole (research)	[76]
500–1000	BLDC (humanoid robot)	[66]
3000–6000	DC (foot prosthesis)	[48]

An analysis of nominal operating speeds reveals a significant dichotomy in drive engineering. A prominent modern trend favors low-speed machines operating between 0 and 1000 RPM. Utilizing these lower speeds enhances the dynamic flexibility and compliance of robotic joints. Conversely, legacy solutions relying on high-speed DC commutator motors (operating at 3000–6000 RPM) remain prevalent, particularly in commercial foot prostheses.

3.9. Machine Nominal Current

An analysis of the rated currents confirms a direct relationship between the required torque and the supply current under limited voltage conditions. For less loaded humanoid robot components, currents in the range of 3–6 A are sufficient. However, the increase in dynamic requirements in more advanced humanoid designs necessitates the use of currents in the range of 18–21 A. The most extreme operating conditions are observed in specialized high-torque drives used in prostheses, where rated currents reach values in the range of 21–60 A. The achieved results of comparison are presented in Table 12.

Table 12. High torque machine nominal currents.

Machine Current [A]	Machine Example	Publication Example
3–6	BLDC (humanoid)	[3]
18–21	BLDC (humanoid robot)	[10]
21–60	Other High Torque (prosthesis)	[65]

3.10. Machine Torque Density

Torque density is arguably the most critical metric for wearable robotics, dictating the ultimate physical weight of the assistive drive. Maximizing this indicator is crucial; any extraneous mass attached to a user's limb exponentially increases their metabolic cost and

rotational inertia, severely disrupting natural gait mechanics. Modern high-efficiency drives target values of several dozen Nm/kg, allowing the mechanical hardware to approach the high-performance thresholds of biological human muscles. The comparison results are summarized in Table 13.

Table 13. High torque machine torque densities.

Range	Unit	Machine Example	Publication Example
0–35	Nm/kg	FSCW (biomimetic robot)	[69]
>35	Nm/kg	Halbach magnetic gearbox (research)	[92]

Analyzing torque density identifies two distinct technological tiers. The first tier, ranging from 0 to 35 Nm/kg, characterizes modern motors in biomimetic robots, frequently utilizing fractional-slot concentrated winding (FSCW) technology. Operating at the upper echelon of this range yields a highly favorable power-to-weight ratio, sufficient for most modern prostheses and lightweight walking robots. Conversely, exceeding the 35 Nm/kg threshold enters the experimental domain, necessitating a departure from classical topologies in favor of cutting-edge research solutions. A prime example is the implementation of magnetic transmissions utilizing Halbach arrays. While these structures achieve extreme magnetic flux concentration and superior torque density, they inevitably introduce severe design complexities and elevated manufacturing costs.

4. Discussion

Despite the theoretical availability of advanced magnetic topologies, the biomechanical market remains heavily dominated by classic BLDC motors. This is primarily due to the exceptional maturity of the technology, the simplicity of control algorithms, and the widespread availability of commercial off-the-shelf components. However, a critical comparison of parameters clearly indicates that these conventional solutions are rapidly approaching their absolute miniaturization limits. Achieving the requisite 60–65 Nm of torque while maintaining a strictly constrained mass below 1200 g forces the integration of high-ratio mechanical gearboxes. This integration severely degrades the system's overall efficiency and severely limits its backdrivability.

The central conclusion derived from this review is the paramount importance of torque density. The analysis exposed a definitive boundary between conventional solutions (0–35 Nm/kg) and experimental architectures (>35 Nm/kg). Breaching the 35 Nm/kg limit—a necessity if prostheses are to truly mimic biological muscle metrics—requires engineers to abandon standard radial-flux designs in favor of specialized topologies, such as magnetic gears or Vernier machines utilizing Halbach arrays. This trajectory suggests that the future of advanced biorobotics lies in the sophisticated integration of unconventional magnetic systems, rather than the mere geometric scaling of legacy DC/BLDC motors.

The dimensional boundaries identified in this study represent more than just assembly constraints; they are the fundamental pillars of anthropomorphic design. Exceeding these physical limits—as demonstrated by the analysis of YASA motors—categorically disqualifies a drive from prosthetic applications, regardless of its exceptional torque characteristics. Designers must continuously navigate these strict volumetric limits, a necessity that heavily incentivizes the research and development of short-stack, axial-flux topologies.

Furthermore, a significant engineering conflict persists between stringent safety regulations and escalating power demands. The industry standard mandates the use of safety extra-low voltage (SELV) power supplies, capped at 48 V. For heavy-duty exoskeletons requiring power outputs exceeding 500 W, this voltage cap forces the system to operate at exceptionally high currents (peaking up to 60 A). These massive currents generate severe

resistive heat losses within the stator windings. In wearable applications, where active liquid cooling is prohibited by rigid weight constraints, this thermal reality places extreme demands on insulation materials and passive heat dissipation strategies.

Finally, a distinct paradigm shift is evident regarding operating velocities: high-speed DC motors (3000–6000 RPM) are gradually being superseded by low-speed architectures (below 1000 RPM). This transition is intrinsically linked to the adoption of Direct Drive (DD) and Quasi-Direct Drive (QDD) philosophies. Eliminating mechanical reduction stages vastly improves the dynamic response and proprioceptive "feel" of the prosthesis interacting with the environment. However, achieving this requires motors with significantly larger diameters or highly specialized flux-modulating designs, thereby cyclically returning the engineering focus back to the core challenge of geometric limitation. Table 14 presents the optimal, desirable parameters for electric machines in biomechanical applications, synthesized from the comprehensive literature review.

Table 14. High torque machines desirable parameters for biomechanical applications based on analysis.

Parameter	Value	Unit
Motor type	BLDC Servo High Torque PMSM	-
Max diameter	150	mm
Max length	85	mm
Max mass	1200	g
Efficiency	$\leq$95	%
Power	even 500	W
Max torque	65	Nm
Voltage	$\leq$48	V
Speed	$\leq$1000	RPM
Current	even 60	A
Torque density	even 45	Nm/kg

Despite the wealth of literature on high-torque electric machines, our review identifies significant research gaps that hinder the standardization of biorobotic drives. First, there is a clear absence of standardized testing platforms; experimental results are often reported using proprietary testbeds, making the comparative assessment of efficiency and thermal performance across different topologies nearly impossible. Second, longitudinal durability data under realistic gait-cycle loading is critically insufficient. Most studies focus on peak torque and efficiency at steady-state conditions, whereas the actual operational life of a biomechanical actuator involves highly stochastic, dynamic stress that current literature fails to characterize adequately. Finally, there is a lack of harmonized metrics for reporting thermal behavior, making it difficult to assess how emerging topologies will perform in thermally constrained, closed-environment wearable applications.

It should be noted that the analyzed electric machine topologies include both commercially established solutions and emerging experimental designs; the latter, while theoretically promising, currently require further validation in real-world prosthetic and exoskeleton applications.

It is critical to acknowledge that geometric and mass constraints are highly dependent on the target anatomical segment. For robotic hands, where fine motor skills are prioritized over raw force, torque requirements are minimal (typically <5 Nm), allowing for highly compact, low-mass designs. In contrast, lower limb applications—specifically knee and ankle joints—impose the most stringent demands; these actuators must operate under high dynamic loads, often requiring torque outputs exceeding 60 Nm. Exoskeletons, due to the need to support the user's entire body weight, represent a distinct category requiring the highest power and torque density metrics, whereas upper-limb prostheses occupy an intermediate position, balancing compactness with moderate force generation.

The reliance on low-voltage DC buses (typically $\leq$48 V) to ensure user safety necessitates high current density, which directly impacts the thermal management of the drive system. In wearable robotics, this creates a critical trade-off: higher currents lead to increased Joule heating within the stator windings and power electronics. Given the limited surface area for heat dissipation in compact, enclosed wearable devices, localized thermal hotspots can significantly degrade the insulation and lifetime of the motor. Furthermore, excessive heat accumulation poses a direct risk to user comfort and safety, necessitating strict thermal design limits that often constrain the continuous torque output of the actuator well below its peak performance capability. Therefore, thermal-aware design and advanced heat-sinking integration are as vital as achieving target torque density in biomechanical applications.

5. Conclusions

This article provides an in-depth analysis of established electric machine designs, meticulously evaluating their applicability within biomechanical constructs. Electric machines serve as the foundational mechanical components of advanced bionic devices, including active prostheses, load-bearing exoskeletons, and humanoid robots, fundamentally dictating their overall functionality and dynamic performance. While conventional motors (primarily BLDC, Servo, and PMSM) successfully generate sufficient shaft torque for many applications, the literature clearly indicates a pressing need for optimization. Alternative high-torque topologies, though currently less ubiquitous in commercial products, possess immense potential to drastically enhance the adaptability and efficiency of future biorobotic systems. These emerging motor architectures offer critical advantages, including superior energy efficiency, reduced mass, and enhanced dynamic flexibility—metrics that are absolutely paramount in the design of modern wearable mechatronics.

Based on the comprehensive quantitative analysis summarized in Table 14, definitive engineering guidelines for anthropomorphic drive systems have been established. To ensure biomechanical compatibility and user ergonomics without compromising performance, the ideal drive unit must fit within a maximum outer diameter of 150 mm and an axial length not exceeding 85 mm. Furthermore, strict mass minimization remains an absolute priority; the isolated motor weight must be maintained below 1200 g to prevent detrimental alterations to the user's natural gait dynamics.

Advanced magnetic topologies are currently achieving highly desirable performance thresholds, specifically demonstrating the capacity to handle nominal currents up to 60 A while delivering exceptional torque density values reaching 45 Nm/kg. Surpassing this specific torque density metric is the critical evolutionary step required for robotic actuators to realistically replicate the performance capabilities of biological human muscles.

These emerging motor designs offer substantial systemic advantages, including outstanding energy efficiency (>95%) and the crucial capability for low-speed, high-torque operation ($\leq$1000 RPM). This directly aligns with the modern biorobotic trend of minimizing or entirely eliminating mechanical transmission ratios. Future scientific research should

prioritize the optimization of these flux-modulating topologies, focusing specifically on balancing high electrical power demands (reaching 500 W) with the strict safety constraints of low-voltage battery systems ($\leq$48 V), which remains the definitive bottleneck in the evolution of wearable biomechanical technology.

It should be noted that the recommended parameter ranges presented in this study are derived from a diverse set of biomechanical applications, ranging from robotic prosthetics to humanoid platforms. Therefore, these values should be treated as practical design guidelines rather than universal technical standards, as specific requirements may vary significantly depending on the target application.

Author Contributions: M.C.: Conceptualization, Writing—original draft, Project administration, Resources, Writing—review and editing. M.W. and P.W.H.: Formal analysis, Resources, Writing—review and editing. All authors have read and agreed to the published version of the manuscript.

Funding: Project financed from state budget funds granted by the Minister of Education and Science within the framework of the "Pearls of Science" programme with the number PN/01/0004/2022, entitled "High torque permanent magnet machine for use in biomechanical structures". Organisational unit implementing the task: Department of Electrical Machines and Drives at the Faculty of Electrical Engineering of the West Pomeranian University of Technology in Szczecin—total funding amount: 228 800.00 PLN.

Data Availability Statement: No new data were created or analyzed in this study.

Conflicts of Interest: The authors declare no conflicts of interest.

References

1. Gao, S.; Mai, J.; Zhu, J.; Wang, Q. Mechanism and Controller Design of a Transfemoral Prosthesis with Electrohydraulic Knee and Motor-Driven Ankle. *IEEE/ASME Trans. Mechatron.* **2021**, *26*, 5. [CrossRef]
2. Bai, S.; Islam, M.; Power, V.; O'Sullivan, L. User-centered development and performance assessment of a modular full-body exoskeleton (AXO-SUIT). *Biomim. Intell. Robot.* **2022**, *2*, 100032. [CrossRef]
3. Ishiguro, Y.; Makabe, T.; Nagamatsu, Y.; Kojio, Y.; Kojima, K.; Sugai, F.; Kakiuchi, Y.; Okada, K.; Inaba, M. Bilateral Humanoid Teleoperation System Using Whole-Body Exoskeleton Cockpit TABLIS. *IEEE Robot. Autom. Lett.* **2020**, *5*, 6419–6426. [CrossRef]
4. Laschowski, B.; McPhee, J. Energy-Efficient Actuator Design Principles for Robotic Leg Prostheses and Exoskeletons: A Review of Series Elasticity and Backdrivability. *J. Comput. Nonlinear Dyn.* **2023**, *18*, 060801. [CrossRef]
5. Kawaharazuka, K.; Makino, S.; Tsuzuki, K.; Onitsuka, M.; Nagamatsu, Y.; Shinjo, K.; Makabe, T.; Asano, Y.; Okada, K.; Kawasaki, K.; et al. Component Modularized Design of Musculoskeletal Humanoid Platform Musashi to Investigate Learning Control Systems. In Proceedings of the 2019 IEEE/RSJ International Conference on Intelligent Robots and Systems (IROS), Macau, China, 3–8 November 2019.
6. Ismawan, A.R.; Ismail, R.; Novriansyah, R.; Setiyana, B.; Ariyanto, M.; Prahasto, T. Conceptual Design of Bionic Foot for Transtibial Prosthesis. In Proceedings of the 2021 IEEE International Biomedical Instrumentation and Technology Conference (IBITeC), Yogyakarta, Indonesia, 20–21 October 2021.
7. Eßer, J.; Kumar, S.; Peters, H.; Bargsten, V.; de Gea Fernandez, J.; Mastalli, C.; Stasse, O.; Kirchner, F. Design, analysis and control of the series-parallel hybrid RH5 humanoid robot. In Proceedings of the 2020 IEEE-RAS 20th International Conference on Humanoid Robots (Humanoids), Munich, Germany, 19–21 July 2021.
8. Bartlett, H.L.; Lawson, B.E.; Goldfarb, M. Design, Control, and Preliminary Assessment of a Multifunctional Semipowered Ankle Prosthesis. *IEEE/ASME Trans. Mechatron.* **2019**, *24*, 1532–1540. [CrossRef]
9. Palay, M.; Sotelo, R. Design of an affordable lower limb bionic prosthesis. In Proceedings of the IEEE Global Humanitarian Technology Conference, Santa Clara, CA, USA, 8–11 September 2022.
10. Wang, S.; Ramos, J. Dynamic Locomotion Teleoperation of a Reduced Model of a Wheeled Humanoid Robot Using a Whole-Body Human-Machine Interface. *IEEE Robot. Autom. Lett.* **2022**, *7*, 1872–1879. [CrossRef]
11. Wang, X.; Meng, Q.; Zhang, Z.; Sun, J.; Yang, J.; Yu, H. Design and evaluation of a hybrid passive–active knee prosthesis on energy consumption. *Mech. Sci.* **2020**, *11*, 425–436. [CrossRef]
12. Camargo, J.; Bhakta, K.; Maldonado-Contreras, J.; Zhou, S.; Herrin, K.; Young, A. OpenSim Model for Biomechanical Analysis with the Open-Source Bionic Leg. In Proceedings of the International Symposium on Medical Robotics (ISMR), Atlanta, GA, USA, 13–15 April 2022.

13. Kang, I.; Kunapuli, P.; Young, A.J. Real-Time Neural Network-Based Gait Phase Estimation Using a Robotic Hip Exoskeleton. *IEEE Trans. Med. Robot. Bionics* **2020**, *2*, 28–37. [CrossRef]
14. You, W.S.; Lee, Y.H.; Oh, H.S.; Kang, G.; Choi, H.R. Design of a 3D-printable, robust anthropomorphic robot hand including intermetacarpal joints. *Intell. Serv. Robot.* **2019**, *12*, 1–16. [CrossRef]
15. Li, H.; Yu, H.; Chen, Y.; Tang, X.; Wang, D.; Meng, Q.; Du, Q. Design of a Minimally Actuated Lower Limb Exoskeleton with Mechanical Joint Coupling. *J. Bionic Eng.* **2022**, *19*, 370–389. [CrossRef]
16. Meijneke, C.; van Oort, G.; Sluiter, V.; van Asseldonk, E.; Tagliamonte, N.L.; Tamburella, F.; Pisotta, I.; Masciullo, M.; Arquilla, M.; Molinari, M.; et al. Symbitron Exoskeleton: Design, Control, and Evaluation of a Modular Exoskeleton for Incomplete and Complete Spinal Cord Injured Individuals. *IEEE Trans. Neural Syst. Rehabil. Eng.* **2021**, *29*, 330–339. [CrossRef]
17. Shao, Y.; Zhang, W.; Su, Y.; Ding, X. Design and optimisation of load-adaptive actuator with variable stiffness for compact ankle exoskeleton. *Mech. Mach. Theory* **2021**, *161*, 104323. [CrossRef]
18. Prathibanandhi, K.; Yaashuwanth, C.; Basha, A.R. Improved torque performance in BLDC-motor-drive through Jaya optimization implemented on Xilinx platform. *Microprocess. Microsyst.* **2021**, *81*, 103681. [CrossRef]
19. Zhang, Z. A Compact High Torque Density Dual Rotor Permanent Magnet In-Wheel Motor with Toroidal Windings. In Proceedings of the 22nd International Conference on Electrical Machines and Systems (ICEMS), Harbin, China, 11–14 August 2019.
20. Ebrahimi, A.; Minzenmay, D.; Budaker, B.; Schneider, U. Bionic Upper Orthotics with Integrated EMG Sensory. In Proceedings of the 23rd IEEE International Symposium on Robot and Human Interactive Communication, Edinburgh, UK, 25–29 August 2014.
21. Yu, S.; Huang, T.-H.; Wang, D.; Lynn, B.; Sayd, D.; Silivanov, V.; Park, Y.S.; Tian, Y.; Su, H. Design and Control of a High-Torque and Highly Backdrivable Hybrid Soft Exoskeleton for Knee Injury Prevention During Squatting. *IEEE Robot. Autom. Lett.* **2019**, *4*, 4579–4586. [CrossRef]
22. Sarkisian, S.V.; Ishmael, M.K.; Hunt, G.R.; Lenzi, T. Design, Development, and Validation of a Self-Aligning Mechanism for High-Torque Powered Knee Exoskeletons. *IEEE Trans. Med. Robot. Bionics* **2020**, *2*, 248–259. [CrossRef]
23. Yang, H.; Wei, G.; Ren, L.; Qian, Z.; Wang, K. A low-cost linkage-spring-tendon-integrated compliant anthropomorphic robotic hand: MCR-Hand III. *Mech. Mach. Theory* **2021**, *158*, 104210. [CrossRef]
24. Unanyan, N.N.; Belov, A.A. Design of upper limb prosthesis using real-time motion detection method based on EMG signal processing. *Biomed. Signal Process. Control* **2021**, *70*, 103062. [CrossRef]
25. Țîmpea, Ș.A.; Cosma, C.; Codrean, C.; Magda, A. Design of a Bionic Arm Using Rapid Prototyping Technology. *Hidraulica* **2019**, *4*, 21–28.
26. Hedayati, H.; Bhaduri, S.; Sumner, T.; Szafir, D.; Gross, M.D. HugBot: A soft robot designed to give human-like hugs. In Proceedings of the 18th ACM International Conference on Interaction Design and Children, Boise, ID, USA, 12–15 June 2019; pp. 556–561.
27. Teyssier, M.; Koelle, M.; Strohmeier, P.; Fruchard, B.; Steimle, J. Eyecam: Revealing Relations between Humans and Sensing Devices through an Anthropomorphic Webcam. In Proceedings of the 2021 CHI Conference on Human Factors in Computing Systems, Yokohama, Japan, 8–13 May 2021; pp. 1–13.
28. Hu, A.; Yin, Q.; Li, Q.; Yang, H.; Zhang, Y. Structure design and kinematics analysis of lower limb rehabilitation training robot. In Proceedings of the 2020 3rd International Conference on E-Business, Information Management and Computer Science, Wuhan, China, 5–6 December 2020; pp. 410–415.
29. Fuentes-Gonzalez, J.; Infante-Alarcon, A.; Asanza, V.; Loayza, F.R. A 3D-Printed EEG based Prosthetic Arm. In Proceedings of the 2020 IEEE International Conference on E-health Networking, Application & Services (HEALTHCOM), Shenzhen, China, 1–2 March 2020.
30. Gabert, L.; Hood, S.; Tran, M.; Cempini, M.; Lenzi, T. A Compact, Lightweight Robotic Ankle-Foot Prosthesis. *IEEE Robot. Autom. Mag.* **2020**, *27*, 87–102. [CrossRef]
31. Puliti, M.; Tessari, F.; Galluzzi, R.; Traverso, S.; Tonoli, A.; Michieli, L.D.; Laffranchi, M. A Hybrid Swing-Assistive Electro-Hydrostatic Bionic Knee Design. In Proceedings of the 9th IEEE RAS/EMBS International Conference for Biomedical Robotics and Biomechatronics (BioRob), Seoul, Republic of Korea, 21–24 August 2022.
32. Bhavani, S.; Krishna, K.; Reddy, R.; Geethika, T. A Low Cost Bionic Arm Based on Electromyography Sensor. In Proceedings of the 7th International Conference on Signal Processing and Integrated Networks (SPIN), Noida, India, 27–28 February 2020.
33. Zhou, H.; Mohammadi, A.; Oetomo, D.; Alici, G. A Novel Monolithic Soft Robotic Thumb for an Anthropomorphic Prosthetic Hand. *IEEE Robot. Autom. Lett.* **2019**, *4*, 602–609. [CrossRef]
34. Hou, F.; Liu, J.; Liu, K.; Chen, D.; Guo, S. A Robotic Lower Limb with Eight DoFs and Whole-Foot Tactile Perception for Anthropomorphic Behavior Performance. In Proceedings of the IEEE International Conference on Robotics and Automation (ICRA), Philadelphia, PA, USA, 23–27 May 2022.
35. Guercini, L.; Driessen, J.; Buccelli, S.; Pace, A.; Giuseppe, S.D.; Traverso, S.; Michieli, L.D.; Laffranchi, M. An Over-Actuated Bionic Knee Prosthesis: Modeling, Design and Preliminary Experimental Characterization. In Proceedings of the IEEE International Conference on Robotics and Automation (ICRA), Philadelphia, PA, USA, 23–27 May 2022.

36. Jing, X.; Yong, X.; Jiang, Y.; Li, G.; Yokoi, H. Anthropomorphic Prosthetic Hand with Combination of Light Weight and Diversiform Motions. *Appl. Sci.* **2019**, *9*, 4203. [CrossRef]
37. Devaraja, R.R.; Maskeliunas, R.; Damaševicius, R. Design and Evaluation of Anthropomorphic Robotic Hand for Object Grasping and Shape Recognition. *Computers* **2021**, *10*, 1. [CrossRef]
38. Vimolmongkolporn, V.; Kato, F.; Handa, T.; Iwasaki, Y.; Iwata, H. Design and development of 6 DoFs detachable robotic head utilizing differential gear mechanism to imitate human head-waist motion. In Proceedings of the 2022 IEEE/SICE International Symposium on System Integration (SII), Narvik, Norway, 9–12 January 2022.
39. Rane, K.P. Design and Development of Low Cost Humanoid Robot with Thermal Temperature Scanner for COVID-19 Virus Preliminary Identification. *Int. J. Adv. Trends Comput. Sci. Eng.* **2020**, *9*, 3485–3493. [CrossRef]
40. Grazi, L.; Trigili, E.; Proface, G.; Giovacchini, F.; Crea, S.; Vitiello, N. Design and Experimental Evaluation of a Semi-Passive Upper-Limb Exoskeleton for Workers with Motorized Tuning of Assistance. *IEEE Trans. Neural Syst. Rehabil. Eng.* **2020**, *28*, 2276–2285. [CrossRef]
41. Dragusanu, M.; Iqbal, M.Z.; Baldi, T.L.; Prattichizzo, D.; Malvezzi, M. Design, Development, and Control of a Hand/Wrist Exoskeleton for Rehabilitation and Training. *IEEE Trans. Robot.* **2022**, *38*, 1472–1488. [CrossRef]
42. Prasad, D.D.; CH, V.K. Structural design of zoomorphic robot. In *IOP Conference Series: Materials Science and Engineering*; IOP Publishing: Bristol, UK, 2020; Volume 912.
43. Kaneko, K.; Kaminaga, H.; Sakaguchi, T.; Kajita, S.; Morisawa, M.; Kumagai, I.; Kanehiro, F. Humanoid Robot HRP-5P: An Electrically Actuated Humanoid Robot with High-Power and Wide-Range Joints. *IEEE Robot. Autom. Lett.* **2019**, *4*, 1431–1438. [CrossRef]
44. Gao, M.; Wang, Z.; Pang, Z.; Sun, J.; Li, J.; Li, S.; Zhang, H. Electrically Driven Lower Limb Exoskeleton Rehabilitation Robot Based on Anthropomorphic Design. *Machines* **2022**, *10*, 266. [CrossRef]
45. Vergaray, R.A.; Aguila, R.F.D.; Avellaneda, G.A.; Palomares, R.; Cornejo, J.; Cornejo-Aguilar, J.A. Mechatronic System Design and Development of iROD: EMG Controlled Bionic Prosthesis for Middle-Third Forearm Amputee. In Proceedings of the IEEE Fifth Ecuador Technical Chapters Meeting (ETCM), Cuenca, Ecuador, 12–15 October 2021.
46. Cano, S.; Díaz, J.; López, J.A.; Libreros, J.E.; García, M. Design path for a Social Robot for Emotional Communication for Children with Autism Spectrum Disorder (ASD). *Sensors* **2023**, *23*, 5291. [CrossRef]
47. Cheng, M.; Han, Z.; Ding, R.; Zhang, J.; Xu, B. Development of a redundant anthropomorphic hydraulically actuated manipulator with a roll–pitch–yaw spherical wrist. *Front. Mech. Eng.* **2021**, *16*, 698–710. [CrossRef]
48. Xu, X.; Xu, X.; Liu, Y.; Zhong, K.; Zhang, H. Design of bionic active–passive hybrid driven prosthesis based on gait analysis and simulation of compound control method. *BioMed. Eng. OnLine* **2021**, *20*, 126. [CrossRef] [PubMed]
49. Li, C.; Gu, X.; Xiao, X.; Zhu, G.; Prituja, A.V.; Ren, H. Transcend Anthropomorphic Robotic Grasping with Modular Antagonistic Mechanisms and Adhesive Soft Modulations. *IEEE Robot. Autom. Lett.* **2019**, *4*, 2463–2470. [CrossRef]
50. Hayosh, D.; Liu, X.; Lee, K. Woody: Low-Cost, Open-Source Humanoid Torso Robot. In Proceedings of the 17th International Conference on Ubiquitous Robots (UR), Kyoto, Japan, 22–26 June 2020.
51. Sivaranjani, A.; Vinod, B.; Vasanthakumar, M. Selection And Implementation Of Electric Drives And Its Control For Mobile Humanoid Robot. *Int. J. Aquat. Sci.* **2021**, *12*, 3970–3979.
52. Zhang, Q.; Zhao, C.; Fan, L.; Zhang, Y. Taikobot: A Full-Size and Free-Flying Humanoid Robot for Intravehicular Astronaut Assistance and Spacecraft Housekeeping. *Machines* **2022**, *10*, 933. [CrossRef]
53. Yu, X.; Fan, Z.; Wang, X.; Wan, H.; Wang, P.; Zeng, X.; Jia, F. A lab-customized autonomous humanoid apple harvesting robot. *Comput. Electr. Eng.* **2021**, *96*, 107459. [CrossRef]
54. Nurpeissova, A.; Tursynbekov, T.; Shintemirov, A. An Open-Source Mechanical Design of ALARIS Hand: A 6-DOF Anthropomorphic Robotic Hand. In Proceedings of the IEEE International Conference on Robotics and Automation (ICRA 2021), Xian, China, 30 May–5 June 2021.
55. Zhang, Y.; Wang, E.; Wang, M.; Liu, S.; Ge, W. Design and Experimental Research of Knee Joint Prosthesis Based on Gait Acquisition Technology. *Biomimetics* **2021**, *6*, 28. [CrossRef]
56. Jiang, J.; Chen, P.; Peng, J.; Qiao, X.; Zhu, F.; Zhong, J. Design and Optimization of Lower Limb Rehabilitation Exoskeleton with a Multiaxial Knee Joint. *Biomimetics* **2023**, *8*, 156. [CrossRef]
57. Masroor, S.; Shah, S.H.; Arsalan, M.; Alam, M.S.; Khan, S.G.; Imran, A. Design and Control of a Bionic Leg. In Proceedings of the 2023 International Multi-disciplinary Conference in Emerging Research Trends (IMCERT), Karachi, Pakistan, 4–5 January 2023.
58. Sun, B.-Y.; Gong, X.; Liang, J.; Chen, W.-B.; Xie, Z.-L.; Liu, C.; Xiong, C.-H. Design Principle of a Dual-Actuated Robotic Hand with Anthropomorphic Self-Adaptive Grasping and Dexterous Manipulation Abilities. *IEEE Trans. Robot.* **2022**, *38*, 2322–2340. [CrossRef]
59. Shah, D.; Wu, Y.; Scalzo, A.; Metta, G.; Parmiggiani, A. A Comparison of Robot Wrist Implementations for the iCub Humanoid. *Robotics* **2019**, *8*, 11. [CrossRef]

60. Kim, U.; Jung, D.; Jeong, H.; Park, J.; Jung, H.-M.; Cheong, J.; Choil, H.R.; Do, H.; Park, C. Integrated linkage-driven dexterous anthropomorphic robotic hand. *Nat. Commun.* **2021**, *12*, 7177. [CrossRef] [PubMed]
61. Szymona, B.; Maciejewski, M.; Karpinski, R.; Jonak, K.; Radzikowska-Büchner, E.; Niderla, K.; Prokopiak, A. Robot-Assisted Autism Therapy (RAAT). Criteria and Types of Experiments Using Anthropomorphic and Zoomorphic Robots. Review of the Research. *Sensors* **2021**, *21*, 3720. [CrossRef] [PubMed]
62. Wu, J.; Guo, L.; Yan, S.; Li, Y.; Yao, Y.-A. Design and performance analysis of a novel closed-chain elastic-bionic leg with one actuated degree of freedom. *Mech. Mach. Theory* **2021**, *165*, 104444. [CrossRef]
63. Widhiada, W.; Nindhia, T.G.T.; Budiarsa, I.N. Design of The Bionic Robot Hand with Electromyography Smart Sensor based on MATLAB/Simulink. *Int. J. Mech. Eng. Robot. Res.* **2020**, *9*, 1122–1127. [CrossRef]
64. Vinoj, P.G.; Jacob, S.; Menon, V.G.; Rajesh, S.; Khosravi, M.R. Brain-Controlled Adaptive Lower Limb Exoskeleton for Rehabilitation of Post-Stroke Paralyzed. *IEEE Access* **2019**, *7*, 132628–132648. [CrossRef]
65. Carney, M.E.; Shu, T.; Stolyarov, R.; Duval, J.-F.; Herr, H.M. Design and Preliminary Results of a Reaction Force Series Elastic Actuator for Bionic Knee and Ankle Prostheses. *IEEE Trans. Med. Robot. Bionics* **2021**, *3*, 542–553. [CrossRef]
66. Chignoli, M.; Kim, D.; Stanger-Jones, E.; Kim, S. The MIT Humanoid Robot: Design, Motion Planning, and Control For Acrobatic Behaviors. In Proceedings of the IEEE-RAS 20th International Conference on Humanoid Robots (Humanoids), Munich, Germany, 19–21 July 2020.
67. Wang, Y.; Zhang, R. Design of Bionic Batfish Based on Topology Optimization Method. In Proceedings of the 7th International Conference on Control, Automation and Robotics ICCAR, Singapore, 23–26 April 2021.
68. Zhang, Z.; Yu, S.; Zhang, F.; Jin, S.; Wang, X. Electromagnetic and Structural Design of a Novel Low-Speed High-Torque Motor with Dual-Stator and PM-Reluctance Rotor. *IEEE Trans. Appl. Supercond.* **2020**, *30*, 4. [CrossRef]
69. Zhang, W.; Yu, Z.; Chen, X.; Huang, Q.; Gao, J.; Zhang, W.; Ming, A.; Zhu, M. Electromagnetic Design of a High Torque Density Permanent Magnet Motor for Biomimetic Robot. In Proceedings of the IEEE International Conference on Cyborg and Bionic Systems, Beijing, China, 17–19 October 2017.
70. Su, H.; Yan, L.; Zhag, L.; Wei, X.; Dong, Z.; Jin, Z. High Torque Density Electrical Machine with Less Rare Earth Permanent Magnet. In Proceedings of the IEEE 17th Conference on Industrial Electronics and Applications (ICIEA), Chengdu, China, 16–19 December 2022.
71. Zhang, Z. High Torque Density Spoke-Type Ferrite Permanent Magnet Synchronous Machine Assisted by Rare-Earth Magnets for Traction Applications. In Proceedings of the IEEE Energy Conversion Congress and Exposition (ECCE), Detroit, MI, USA, 11–15 October 2020.
72. Baloch, N.; Kwon, B.-i.; Gao, Y. Low-Cost High-Torque-Density Dual-Stator Consequent-Pole Permanent Magnet Vernier Machine. *IEEE Trans. Magn.* **2018**, *54*, 11. [CrossRef]
73. Wang, W.; Ma, H.; Qiu, X.; Yang, J. A Calculation Method for the On-Load Cogging Torque of Permanent Magnet Synchronous Machine. *IEEE Access* **2019**, *7*, 106316–106326. [CrossRef]
74. Sayed, E.; Yang, Y.; Bilgin, B.; Bakr, M.H.; Emadi, A. A Comprehensive Review of Flux Barriers in Interior Permanent Magnet Synchronous Machines. *IEEE Access* **2019**, *7*, 149168–149181. [CrossRef]
75. Wong, H.Y.; Bird, J.Z.; Barnett, D.; Williams, W. A High Torque Density Halbach Rotor Coaxial Magnetic Gear. In Proceedings of the IEEE International Electric Machines & Drives Conference (IEMDC), San Diego, CA, USA, 12–15 May 2019.
76. Liang, J.; Parsapour, A.; Cosoroaba, E.; Wu, M.; Boldea, I.; Fahimi, B. A High Torque Density Outer Rotor Claw Pole Stator Permanent Magnet Synchronous Motor. In Proceedings of the IEEE Transportation Electrification Conference and Expo (ITEC), Long Beach, CA, USA, 13–15 June 2018.
77. Xu, L.; Zhao, W.; Liu, G.; Ji, J.; Niu, S. A Novel Dual-Permanent-Magnet-Excited Machine with Non-Uniformly Distributed Permanent-Magnets and Flux Modulation Poles on the Stator. *IEEE Trans. Veh. Technol.* **2020**, *69*, 7104–7115. [CrossRef]
78. Chen, Q.; Xu, G.; Zhai, F.; Liu, G. A Novel Spoke-Type PM Motor with Auxiliary Salient Poles for Low Torque Pulsation. *IEEE Trans. Ind. Electron.* **2020**, *67*, 4762–4773. [CrossRef]
79. Ibrahim, M.; Bernier, F.; Lamarre, J.-M. A Novel Toroidal Permanent Magnet Motor Structure with High Torque Density and Enhanced Cooling. In Proceedings of the IEEE Energy Conversion Congress and Exposition (ECCE), Detroit, MI, USA, 11–15 October 2020.
80. Chen, Z.; Li, G. A V Type Permanent Magnet Motor Simulation Analysis and Prototype Test for Electric Vehicle. *IEEE Access* **2019**, *7*, 174839–174846. [CrossRef]
81. Dhulipati, H.; Ghosh, E.; Mukundan, S.; Korta, P.; Tjong, J.; Kar, N.C. Advanced Design Optimization Technique for Torque Profile Improvement in Six-Phase PMSM Using Supervised Machine Learning for Direct-Drive EV. *IEEE Trans. Energy Convers.* **2019**, *34*, 2041–2051. [CrossRef]
82. Lee, J.-G.; Lim, D.-K.; Jung, H.-K. Analysis and Design of Interior Permanent Magnet Synchronous Motor Using a Sequential-Stage Magnetic Equivalent Circuit. *IEEE Trans. Magn.* **2019**, *55*, 10. [CrossRef]

83. Zhang, B.; Gan, B.; Li, Q. Analysis of a Fault-Tolerant Module-Combined Stator Permanent Magnet Synchronous Machine. *IEEE Access* **2020**, *8*, 70438–70452. [CrossRef]
84. Du, Z.S.; Lipo, T.A. Cost-Effective High Torque Density Bi-Magnet Machines Utilizing Rare Earth and Ferrite Permanent Magnets. *IEEE Trans. Energy Convers.* **2020**, *35*, 1577–1584. [CrossRef]
85. Zhang, J.; Zhang, B.; Feng, G.; Gan, B. Design and Analysis of a Low-Speed and High-Torque Dual-Stator Permanent Magnet Motor with Inner Enhanced Torque. *IEEE Access* **2020**, *8*, 182984–182995. [CrossRef]
86. Gong, C.; Deng, F. Design and Optimization of a High-Torque-Density Low-Torque-Ripple Vernier Machine Using Ferrite Magnets for Direct-Drive Applications. *IEEE Trans. Ind. Electron.* **2022**, *69*, 5421–5431. [CrossRef]
87. Baninajar, H.; Modaresahmadi, S.; Wong, H.Y.; Bird, J.; Williams, W.; Dechant, B. Designing a Halbach Rotor Magnetic Gear for a Marine Hydrokinetic Generator. *IEEE Trans. Ind. Appl.* **2022**, *58*, 6069–6080. [CrossRef]
88. Li, K.; Modaresahmadi, S.; Williams, W.B.; Bird, J.Z.; Wright, J.D.; Barnett, D. Electromagnetic Analysis and Experimental Testing of a Flux Focusing Wind Turbine Magnetic Gearbox. *IEEE Trans. Energy Convers.* **2019**, *34*, 1512–1521. [CrossRef]
89. Shi, Y.; Jian, L. A Novel Dual-Permanent-Magnet-Excited Machine with Flux Strengthening Effect for Low-Speed Large-Torque Applications. *Energies* **2018**, *11*, 153. [CrossRef]
90. Gao, C.; Gao, M.; Si, J.; Hu, Y.; Gan, C. A Novel Direct-Drive Permanent Magnet Synchronous Motor with Toroidal Windings. *Energies* **2019**, *12*, 432. [CrossRef]
91. Jo, I.-H.; Lee, J.; Lee, H.-W.; Lee, J.-B.; Lim, J.-H.; Kim, S.-H.; Park, C.-B. A Study on MG-PMSM for High Torque Density of 45 kW–Class Tram Driving System. *Energies* **2022**, *15*, 1749. [CrossRef]
92. Wong, H.Y.; Baninajar, H.; Dechant, B.W.; Southwick, P.; Bird, J.Z. Experimentally Testing a Halbach Rotor Coaxial Magnetic Gear with 279 Nm/L Torque Density. *IEEE Trans. Energy Convers.* **2023**, *38*, 507–518. [CrossRef]
93. Chen, H.; EL-Refaie, A.M.; Demerdash, N.A.O. Flux-Switching Permanent Magnet Machines: A Review of Opportunities and Challenges—Part I: Fundamentals and Topologies. *IEEE Trans. Energy Convers.* **2020**, *35*, 684–698. [CrossRef]
94. Du, Z.S.; Lipo, T.A. High Torque Density and Low Torque Ripple Shaped-Magnet Machines Using Sinusoidal Plus Third Harmonic Shaped Magnets. *IEEE Trans. Ind. Appl.* **2019**, *55*, 2601–2610. [CrossRef]
95. Gorginpour, H. Dual-stator consequent-pole Vernier PM motor with improved power factor. *IET Electr. Power Appl.* **2018**, *13*, 652–661. [CrossRef]
96. Ren, Y.; Zhu, Z.Q.; Green, J.E.; Li, Y.; Zhu, S.; Li, Z. Improved Duty-Ratio-Based Direct Torque Control for Dual Three-Phase Permanent Magnet Synchronous Machine Drives. *IEEE Trans. Ind. Appl.* **2019**, *55*, 5843–5853. [CrossRef]
97. Montonen, J.; Montonen, J.; Polikarpova, M.; Pyrhönen, J. Integration Principles and Thermal Analysis of an Oil-Cooled and -Lubricated Permanent Magnet Motor Planetary Gearbox Drive System. *IEEE Access* **2019**, *7*, 69108–69118. [CrossRef]
98. Zhang, Z. Design of Direct Drive Modular Permanent Magnet Generator with Magnetic Slot Wedges and Step Skewed Outer Rotor for Wind Power Applications. In Proceedings of the International Conference on Intelligent Green Building and Smart Grid (IGBSG2019), Yichang, China, 6–9 September 2019.
99. Lu, E.; Li, W.; Yang, X.; Liu, Y. Anti-disturbance speed control of low-speed high-torque PMSM based on second-order non-singular terminal sliding mode load observer. *ISA Trans.* **2019**, *88*, 142–152. [CrossRef]
100. Wei, L.; Nakamura, T. A Novel Dual-Stator Hybrid Excited Permanent Magnet Vernier Machine with Halbach-Array PMs. *IEEE Trans. Magn.* **2021**, *57*, 1–5. [CrossRef]
101. Allahyari, A.; Torkaman, H. A Novel High-Performance Consequent Pole Dual Rotor Permanent Magnet Vernier Machine. *IEEE Trans. Energy Convers.* **2020**, *35*, 1238–1246. [CrossRef]
102. Xu, L.; Zhao, W.; Li, R.; Niu, S. Analysis of Rotor Losses in Permanent Magnet Vernier Machines. *IEEE Trans. Ind. Electron.* **2022**, *69*, 1224–1234. [CrossRef]
103. Wu, F.; El-Refaie, A.M. Permanent magnet vernier machine: A review. *IET Electr. Power Appl.* **2019**, *13*, 127–137. [CrossRef]
104. Dobzhanskyi, O.; Hossain, E.; Amiri, E.; Gouws, R.; Grebenikov, V.; Mazurenko, L.; Pryjmak, M.; Gamaliia, R. Axial-Flux PM Disk Generator with Magnetic Gear for Oceanic Wave Energy Harvesting. *IEEE Access* **2019**, *7*, 44813–44822. [CrossRef]
105. Pyo, H.-J.; Jeong, J.W.; Yu, J.; Lee, S.G.; Kim, W.-H. Design of 3D-Printed Hybrid Axial-Flux Motor Using 3D-Printed SMC Core. *IEEE Trans. Appl. Supercond.* **2020**, *30*, 4. [CrossRef]
106. Praslicka, B.; Johnson, M.; Gardner, M.C.; Dangtran, E.; Toliyat, H.A. Effects of Axial Flux Magnetic Gear Misalignment. In Proceedings of the IEEE Energy Conversion Congress and Exposition (ECCE), Detroit, MI, USA, 11–15 October 2020.
107. Geng, W.; Zhang, Z.; Li, Q. High Torque Density Fractional-Slot Concentrated-Winding Axial-Flux Permanent-Magnet Machine with Modular SMC Stator. *IEEE Trans. Ind. Appl.* **2020**, *56*, 3691–3699.
108. Farahani, E.F.; Kondelaji, M.A.J.; Mirsalim, M. A New Exterior-Rotor Multiple Teeth Switched Reluctance Motor with Embedded Permanent Magnets for Torque Enhancement. *IEEE Trans. Magn.* **2020**, *56*, 1–5. [CrossRef]
109. Davarpanah, G.; Faiz, J. A Novel Structure of Switched Reluctance Machine with Higher Mean Torque and Lower Torque Ripple. *IEEE Trans. Energy Convers.* **2020**, *35*, 1859–1867. [CrossRef]

110. Farahani, E.F.; Kondelaj, M.A.J.; Mirsalim, M. An Innovative Hybrid-Excited Multi-Tooth Switched Reluctance Motor for Torque Enhancement. *IEEE Trans. Ind. Electron.* **2021**, *68*, 982–992. [CrossRef]
111. Xie, H.; Li, Z.; Li, F. Bionics Design of Artificial Leg and Experimental Modeling Research of Pneumatic Artificial Muscles. *J. Robot.* **2020**, *2020*, 3481056. [CrossRef]
112. Wu, L.; Zhu, J.; Fang, Y. A Novel Doubly-Fed Flux-Switching Permanent Magnet Machine with Armature Windings Wound on Both Stator Poles and Rotor Teeth. *IEEE Trans. Ind. Electron.* **2020**, *67*, 10223–10232. [CrossRef]
113. Li, H.; Zhu, Z.Q. Influence of Adjacent Teeth Magnet Polarities on the Performance of Flux Reversal Permanent Magnet Machine. *IEEE Trans. Ind. Appl.* **2019**, *55*, 354–365. [CrossRef]
114. Yang, H.; Zhu, Z.Q.; Lin, H.; Li, H.; Lyu, S. Analysis of Consequent-Pole Flux Reversal Permanent Magnet Machine with Biased Flux Modulation Theory. *IEEE Trans. Ind. Electron.* **2020**, *67*, 2107–2121. [CrossRef]
115. Kwon, J.-W.; Baloch, N.; Kwon, B.-I. High Gear Ratio Flux Switching Permanent Magnet Machine for High Torque Performance. *IEEE Access* **2020**, *8*, 121630–121636. [CrossRef]
116. Shabestari, P.M.; Mehrizi-Sani, A. Current Limiting and Torque Pulsation Reduction of the Induction Motors. In Proceedings of the IEEE Power & Energy Society General Meeting (PESGM), Atlanta, GA, USA, 4–8 August 2019.
117. Arabul, F.K.; Senol, I.; Oner, Y. Performance Analysis of Axial-Flux Induction Motor with Skewed Rotor. *Energies* **2020**, *13*, 4991. [CrossRef]
118. Arish, N.; Teymoori, V.; Yaghobi, H.; Moradi, M. Design of New Linear Vernier Machine with Skew and Halbach Permanent Magnet for Wave Energy Converters. In Proceedings of the 34th International Power System Conference (PSC2019), Teheran, Iran, 9–11 December 2019.
119. Bao, Y.; Degano, M.; Wang, S.; Chuan, L.; Zhang, H.; Xu, Z.; Gerada, C. A Novel Concept of Ribless Synchronous Reluctance Motor for Enhanced Torque Capability. *IEEE Trans. Ind. Electron.* **2020**, *67*, 2553–2563. [CrossRef]
120. Winterborne, D.; Stannard, N.; Sjöberg, L.; Atkinson, G. An Air-Cooled YASA Motor for in-Wheel Electric Vehicle Applications. *IEEE Trans. Ind. Appl.* **2020**, *56*, 6448–6455. [CrossRef]
121. Brack, R.; Amalu, E.H. A review of technology, materials and R&D challenges of upper limb prosthesis for improved user suitability. *J. Orthop.* **2021**, *23*, 88–96. [CrossRef]
122. Koopman, A.S.; Kingma, I.; de Looze, M.P.; van Dieën, J.H. Effects of a passive back exoskeleton on the mechanical loading of the low-back during symmetric lifting. *J. Biomech.* **2020**, *102*, 109486. [CrossRef] [PubMed]
123. Yan, Z.; Han, B.; Du, Z.; Huang, T.; Bai, O.; Peng, A. Development and testing of a wearable passive lower-limb support exoskeleton to support industrial workers. *Biocybern. Biomed. Eng.* **2021**, *41*, 221–238. [CrossRef]
124. Huang, K.; Xian, Y.; Zhen, S.; Sun, H. Robust control design for a planar humanoid robot arm with high strength composite gear and experimental validation. *Mech. Syst. Signal Process.* **2021**, *155*, 107442. [CrossRef]
125. Liu, Y.; Jiang, D.; Tao, B.; Qi, J.; Jiang, G.; Yun, J.; Huang, L.; Li, G. Grasping posture of humanoid manipulator based. *Alex. Eng. J.* **2022**, *61*, 3959–3969. [CrossRef]
126. Harmon, F.; Brăilenau, P.I. Rapid prototyping of a custom upper limb bionic prosthesis. *J. Ind. Des. Eng. Graph.* **2020**, *15*, 35–39.
127. Song, Y. Building a 'Deeper' Trust: Mapping the Facial Anthropomorphic Trustworthiness in Social Robot Design through Multidisciplinary Approaches. *Des. J.* **2020**, *23*, 639–649. [CrossRef]
128. Liu, X.; Zhao, Y.; Geng, D.; Chen, S.; Tan, X.; Cao, C. Soft Humanoid Hands with Large Grasping Force Enabled by Flexible Hybrid Pneumatic Actuators. *Soft Robot.* **2020**, *8*, 175–185. [CrossRef] [PubMed]
129. Głowiński, S.; Ptak, M. A kinematic model of a humanoid lower limb exoskeleton. *Acta Bioeng. Biomech.* **2022**, *24*, 145–157. [CrossRef]
130. Polishchuk, M.; Tkach, M. Mobile Robot with an Anthropomorphic Walking Device: Design and Simulation. *FME Trans.* **2020**, *48*, 13–20. [CrossRef]
131. Ayman, A.; Sabry, M. A Novel Power-optimized CMOS sEMG Device with Ultra Low-noise integrated with ConvNet (VGG16) for Biomedical Applications. *arXiv* **2023**, arXiv:2301.09570. [CrossRef]
132. Kazerooni, H.; Tung, W.; Pillai, M. Evaluation of Trunk-Supporting Exoskeleton. In *Proceedings of the Human Factors and Ergonomics Society Annual Meeting*; SAGE Publications: Los Angeles, CA, USA, 2019.
133. Said, S.; Sheikh, M.; Al-Rashidi, F.; Lakys, Y.; Beyrouthy, T.; Alkork, S. A Customizable Wearable Robust 3D Printed Bionic Arm: Muscle Controlled. In Proceedings of the 3rd International Conference on Bio-Engineering for Smart Technologies (BioSMART), Paris, France, 24–26 April 2019.
134. Kojima, K.; Kojio, Y.; Ishikawa, T.; Sugai, F.; Kakiuchi, Y.; Okada, K.; Inaba, M. A Robot Design Method for Weight Saving Aimed at Dynamic Motions: Design of Humanoid JAXON3-P and Realization of Jump Motions. In Proceedings of the IEEE-RAS 19th International Conference on Humanoid Robots (Humanoids), Toronto, ON, Canada, 15–17 October 2019.
135. Zhou, J.; Chen, X.; Chang, U.; Lu, J.-T.; Leung, C.C.Y.; Chen, Y.; Hu, Y. A Soft-Robotic Approach to Anthropomorphic Robotic Hand Dexterity. *IEEE Access* **2019**, *7*, 101483–101495. [CrossRef]

136. Pacifico, I.; Scano, A.; Guanziroli, E.; Moisé, M.; Morelli, L.; Chiavenna, A.; Romo, D.; Spada, S.; Colombina, G.; Molteni, F.; et al. An Experimental Evaluation of the Proto-MATE. *IEEE Robot. Autom. Mag.* **2020**, *27*, 54–65. [CrossRef]
137. Orekhov, G.; Fang, Y.; Luque, J.; Lerner, Z.F. Ankle Exoskeleton Assistance Can Improve Over-Ground Walking Economy in Individuals with Cerebral Palsy. *IEEE Trans. Neural Syst. Rehabil. Eng.* **2020**, *28*, 461–467. [CrossRef] [PubMed]
138. Xiao, Y.; Ji, X.; Wu, H.; Zhai, X.; Fu, X.; Zhao, J. Bionic Knee Joint Structure and Motion Analysis of a Lower Extremity Exoskeleton. In Proceedings of the 4th International Conference on Robotics and Automation Sciences, Wuhan, China, 14–16 June 2020.
139. Choi, Y.; Choi, M.; Oh, M.; Kim, S. Service robots in hotels: Understanding the service quality perceptions of human-robot interaction. *J. Hosp. Mark. Manag.* **2019**, *29*, 613–635. [CrossRef]
140. Yusof, K.H.; Zulkipli, M.A.; Ahmad, A.S.; Firdaus, M.; Al-Zubaidi, S.; Mohammed, M.N. Design and Development of Prosthetic Leg with a Mechanical System. In Proceedings of the 2021 IEEE 12th Control and System Graduate Research Colloquium (ICSGRC 2021), Shah Alam, Malaysia, 7 August 2021.
141. Yandell, M.B.; Tacca, J.R.; Zelik, K.E. Design of a Low Profile, Unpowered Ankle Exoskeleton That Fits Under Clothes: Overcoming Practical Barriers to Widespread Societal Adoption. *IEEE Trans. Neural Syst. Rehabil. Eng.* **2019**, *27*, 712–723. [CrossRef]
142. Marquez, J.S.C.; Portilla, C.C.D.l. Design of transtibial mechanical prosthesis with feedback to ground irregularities. In Proceedings of the IEEE 2nd International Congress of Biomedical Engineering and Bioengineering, Bogotá, Colombia, 13–15 October 2021.
143. Dong, X.; Wu, J.; Yin, Z.; Li, X. Development of an intelligent bionic robot rat. In Proceedings of the 2022 IEEE International Conference on Cyborg and Bionic Systems, Wuhan, China, 24–26 March 2023.
144. de Vries, A.W.; Krause, F.; de Looze, M.P. The effectivity of a passive arm support exoskeleton in reducing muscle activation and perceived exertion during plastering activities. *Ergonomics* **2021**, *64*, 712–721. [CrossRef]
145. Fleming, A.; Stafford, N.; Huang, S.; Hu, X.; Ferris, D.P.; Huang, H. Myoelectric control of robotic lower limb prostheses: A review of electromyography interfaces, control paradigms, challenges and future directions. *J. Neural Eng.* **2021**, *18*, 041004. [CrossRef] [PubMed]
146. Liu, C.; Zhang, T.; Zhang, C.; Liu, M.; Chen, Q. Foot Placement Compensator Design for Humanoid Walking Based on Discrete Control Lyapunov Function. *IEEE Trans. Syst. Man Cybern. Syst.* **2021**, *51*, 2332–2341. [CrossRef]
147. Casey, D.; Barrett, E.; Kovacic, T.; Sancarlo, D.; Ricciardi, F.; Murphy, K.; Koumpis, A.; Santorelli, A.; Gallagher, N.; Whelan, S. The Perceptions of People with Dementia and Key Stakeholders Regarding the Use and Impact of the Social Robot MARIO. *Int. J. Environ. Res. Public Health* **2020**, *17*, 8621. [CrossRef]
148. Schellin, H.; Oberley, T.; Patterson, K.; Kim, B.; Haring, K.S.; Tossell, C.C.; Phillips, E.; de Visser, E.J. Man's New Best Friend? Strenghtning Human-Robot Dog Bonding by Enhancing the Doglikeness of Sony's Aibo. In Proceedings of the Systems and Information Engineering Design Symposium (SIEDS), Charlottesville, VA, USA, 24 April 2020.
149. Zhang, J.; Chang, X.; Wang, J.; Chen, W. Mechanical Design and Simulation on Bionic Lower Extremity Rehabilitation Robot. In Proceedings of the 14th IEEE Conference on Industrial Electronics and Applications (ICIEA), Xi'an, China, 19–21 June 2019.
150. Hashimoto, K. Mechanics of humanoid robot. *Adv. Robot.* **2020**, *34*, 1390–1397. [CrossRef]
151. Cornejo, J.; Huamanchahua, D.; Huamán-Vizconde, S.; Terrazas-Rodas, D.; Sierra-Huertas, J.; Janampa-Espinoza, A.; Gonzáles, J.; Cardona, M. Mechatronic Exoskeleton Systems for Supporting the Biomechanics of Shoulder-Elbow-Wrist: An Innovative Review. In Proceedings of the IEEE International IOT, Electronics and Mechatronics Conference (IEMTRONICS), Toronto, ON, Canada, 21–24 April 2021.
152. Yu, J.; Zhang, S.; Wang, A.; Li, W.; Song, L. Musculoskeletal modeling and humanoid control of robots based on human gait data. *PeerJ Comput. Sci.* **2021**, *7*, e657. [CrossRef]
153. Zhou, T.; Xiong, C.; Zhang, J.; Chen, W.; Huang, X. Regulating Metabolic Energy Among Joints During Human Walking Using a Multiarticular Unpowered Exoskeleton. *IEEE Trans. Neural Syst. Rehabil. Eng.* **2021**, *29*, 662–672. [CrossRef]
154. Baltrusch, S.J.; van Dieën, J.H.; Koopman, A.S.; Näf, M.B.; Rodriguez Guerrero, C.; Babič, J.; Houdijk, H. SPEXOR passive spinal exoskeleton decreases metabolic cost during symmetric repetitive lifting. *Eur. J. Appl. Physiol.* **2020**, *120*, 401–412. [CrossRef]
155. Arunkumar, S.; Mahesh, S.; Rahul, M.; Ganesh, N.; Maheshwaran, K.J. Design and analysis of lower limb exoskeleton with external payload. *Int. J. Interact. Des. Manuf.* **2023**, *17*, 2055–2072. [CrossRef]
156. Díaz-Boladeras, M. Bond formation with pet-robots: An integrative approach. *Curr. Psychol.* **2023**, *42*, 2591–2608. [CrossRef]
157. Wood, L.J.; Zaraki, A.; Robins, B.; Dautenhahn, K. Developing Kaspar: A Humanoid Robot for Children with Autism. *Int. J. Soc. Robot.* **2021**, *13*, 491–508. [CrossRef]
158. Ghafurian, M.; Lakatos, G.; Dautenhahn, K. The Zoomorphic Miro Robot's Affective Expression Design and Perceived Appearance. *Int. J. Soc. Robot.* **2022**, *14*, 945–962. [CrossRef]
159. Xu, D.; Li, X.; Wang, Y. Bionic design of universal gripper for nursing robot with hybrid joints and variable Equivalent Link Length. *J. Braz. Soc. Mech. Sci. Eng.* **2022**, *44*, 600. [CrossRef]

160. Jin, J.; Wang, K.; Ren, L.; Qian, Z.; Liang, W.; Xu, X.; Zhao, S.; Lu, X.; Zhao, D.; Wang, X.; et al. Design of a Flexible Bionic Ankle Prosthesis Based on Subject specific Modeling of the Human Musculoskeletal System. *J. Bionic Eng.* **2023**, *20*, 1008–1020. [CrossRef]
161. Yevsieiv, V.; Starikova, S. Analysis of Existing Zoomorphic Mobile Fish Robots. In Proceedings of the Manufacturing & Mechatronic Systems 2022: VIst International Conference, Kharkiv, Ukraine, 21–22 October 2022; pp. 36–38.
162. Chen, Y.; Cai, T.; Zhu, X.; Fan, D.; Wang, Q. Analysis and Design of a New Type of Less-Rare-Earth Hybrid-Magnet Motor with Different Rotor Topologies. *IEEE Trans. Appl. Supercond.* **2020**, *30*, 4. [CrossRef]

Disclaimer/Publisher's Note: The statements, opinions and data contained in all publications are solely those of the individual author(s) and contributor(s) and not of MDPI and/or the editor(s). MDPI and/or the editor(s) disclaim responsibility for any injury to people or property resulting from any ideas, methods, instructions or products referred to in the content.